

Learning High-dimensional Latent Variable Models via Doubly Stochastic Optimisation by Unadjusted Langevin

Motonori Oka, Yunxiao Chen, and Irimi Moustaki

Department of Statistics,
London School of Economics and Political Science

Abstract

Latent variable models are widely used in social and behavioural sciences, such as education, psychology, and political science. In recent years, high-dimensional latent variable models have become increasingly common for analysing large and complex data. Estimating high-dimensional latent variable models using marginal maximum likelihood is computationally demanding due to the complexity of integrals involved. To address this challenge, stochastic optimisation, which combines stochastic approximation and sampling techniques, has been shown to be effective. This method iterates between two steps – (1) sampling the latent variables from their posterior distribution based on the current parameter estimate, and (2) updating the fixed parameters using an approximate stochastic gradient constructed from the latent variable samples. In this paper, we propose a computationally more efficient stochastic optimisation algorithm. This improvement is achieved through the use of a minibatch of observations when sampling latent variables and constructing stochastic gradients, and an unadjusted Langevin sampler that utilises the gradient of the negative complete-data log-likelihood to sample latent variables. Theoretical results are established for the proposed algorithm, showing that the iterative parameter update converges to the marginal maximum likelihood estimate as the number of iterations goes to infinity. Furthermore, the proposed algorithm is shown to scale well to high-dimensional settings through simulation studies and a personality test application with 30,000 respondents, 300 items, and 30 latent dimensions.

KEYWORDS: Langevin diffusion, stochastic approximation, minibatch, Markov chain Monte Carlo, marginal likelihood, empirical Bayes

1 Introduction

Latent variable models are widely used in social and behavioural sciences, such as, education, psychology, and political science ([Bartholomew et al., 2008](#)). In recent years, models with many

latent variables have emerged for analysing large and complex data. Examples include non-linear factor models for large-scale item response data (e.g., [Cai, 2010a; 2010b; Schilling & Bock, 2005](#)) and collaborative filtering (e.g., [Zhu et al., 2016](#)), dynamic factor models for intensive longitudinal data (e.g., [Chen & Zhang, 2020; Chow et al., 2016; Lu et al., 2015](#)), latent space models for network data (e.g., [Hoff et al., 2002](#)), and multilevel models (e.g., [Skrondal & Rabe-Hesketh, 2004](#)). Statistical inference for these models is computationally challenging due to the involvement of many latent variables.

The Marginal Maximum Likelihood Estimator (MMLE) is a popular approach for estimating latent variable models (Chapter 6, [Skrondal & Rabe-Hesketh, 2004](#)), alongside full Bayesian estimation (e.g., [Edwards, 2010](#)) and joint maximum likelihood estimation (e.g., [Chen et al., 2019; 2020; Haberman, 1977](#)). The marginal likelihood approach considers the latent variables as random and unknown parameters as fixed. The likelihood function is obtained from the marginal distribution of the observed data, integrating out the latent variables. This integration poses computational challenges, especially when the latent dimension is high. In particular, the Expectation Maximisation (EM) algorithm ([Bock & Aitkin, 1981; Dempster et al., 1977](#)), often used for optimising the marginal likelihood, becomes computationally infeasible in high-dimensional settings. The EM algorithm alternates between an Expectation (E) step and a Maximisation (M) step. In the E-step, an objective function is constructed at the current parameter estimate, while the M-step updates the parameter estimate by maximising this objective function. The objective function constructed in the E-step involves numerical integrals of the latent variables under their posterior distribution determined by the current parameter estimate. The complexity of this objective function grows exponentially with the latent dimension, making both the E and M steps computationally infeasible in high-dimensional settings.

Several methods have been proposed for optimising marginal likelihoods involving high-dimensional integrals. One line of research approximates the integrals through analytical methods. A well-known method is the Laplace approximation ([Andersson & Xin, 2021; Andersson et al., 2023; Huber et al., 2004; Shun & McCullagh, 1995](#)). This method involves two steps: (1) approximating the integrals in the marginal likelihood using the Laplace approximation at the current parameter values and (2) estimating the unknown parameters based on the approximated likelihood. While the Laplace approximation methods have shown good performance in many settings (e.g., [Andersson & Xin, 2021; Andersson et al., 2023; Shun, 1997](#)), they have two limitations that may limit their applicability for more complex latent variable models. First, Laplace approximation methods do not guarantee the monotone increase of an objective function and, thus, do not necessarily converge. Second, the Laplace approximation results in an approximation error, which propagates to the final estimate. This error does not decay to zero even if the number of iterations or the sample size goes to infinity. Another approach is the adaptive quadrature EM algorithm ([Schilling & Bock, 2005](#)), which approximates the integrals in the E-step of the EM algorithm

using adaptive quadrature points based on a Gaussian approximation. This method has similar limitations as the Laplace approximation.

Another approach involves variants of the EM algorithm that use Markov chain Monte Carlo (MCMC) methods to approximate the integrals in the E-step. Methods in this direction include the Monte Carlo EM algorithm (Meng & Schilling, 1996; Wei & Tanner, 1990) and the Stochastic EM (StEM) algorithm (Diebolt & Ip, 1995; Nielsen & Nielsen, 2000; Zhang et al., 2020). The Monte Carlo EM replaces the numerical integration in the classical EM algorithm with a Monte Carlo integration, where samples of latent variables are generated by MCMC methods. However, the Monte Carlo integration introduces Monte Carlo errors to the parameter estimate in the M-step. This Monte Carlo error decays to zero only when the number of Monte Carlo samples grows to infinity. Thus, the convergence to the MMLE requires the number of Monte Carlo samples to grow with the number of iterations. Thus, this approach can be computationally infeasible when a low Monte Carlo error tolerance is required. The StEM algorithm uses a similar idea but tends to be computationally more efficient. It only uses a small number of Monte Carlo samples in each iteration and then reduces the Monte Carlo error by averaging the parameter trajectory over the iterations. Convergence to the MMLE is guaranteed as the number of iterations converges to infinity (Nielsen & Nielsen, 2000).

The third direction involves stochastic optimisation methods that combine the stochastic approximation (Robbins & Monro, 1951) and sampling techniques. Developments in this direction include Gu and Kong (1998), Cai (2010b), Cai (2010a), Atchade et al. (2017), De Bortoli et al. (2021), and Zhang and Chen (2022). These methods are closely related to the StEM algorithm. They iterate between a sampling step and a stochastic gradient update step. The sampling step is the same as that of the StEM algorithm, though the specific samplers may differ. In this step, a small number of posterior samples of the latent variables are generated, typically via an MCMC sampler. The stochastic gradient update step plays a similar role as the M-step in StEM. However, instead of optimising an objective function constructed by Monte Carlo samples, the stochastic gradient update step performs a one-step update on the parameters along a direction determined by the gradient of the same objective function. This update is known as stochastic approximation. As shown via a simulation study in Zhang and Chen (2022), the stochastic optimisation approach is computationally more efficient than StEM, as performing a stochastic gradient update is substantially faster than solving an optimisation. Among the developments in this direction, we draw attention to the Stochastic Optimisation by Unadjusted Langevin (SOUL) method proposed in De Bortoli et al. (2021), which adopts an Unadjusted Langevin Sampler (ULS; Durmus & Moulines, 2019; Roberts & Tweedie, 1996) in the sampling step. The sampler is an inexact MCMC sampler. It proceeds similarly to an MCMC sampler, but the invariant distribution of its Markov kernel slightly deviates from the target distribution in a controlled way. Compared with the classical MCMC samplers in the other works, such as the random walk Metropolis-Hastings sampler (e.g.,

Cai, 2010a; 2010b) and the Gibbs sampler (e.g., Zhang & Chen, 2022), this sampler can generate approximate samples more efficiently especially in the high-dimensional setting and, thus, may yield more efficient stochastic optimisation. The key to the ULS is the construction of the Markov kernel based on the gradient of the negative log-joint density of observed data and latent variables, utilising the geometric information of the target distribution to improve the sampling efficiency.

This paper proposes a new stochastic optimisation algorithm with two main objectives. Firstly, we aim to bring attention to the SOUL algorithm within the psychometric community, as we believe it can substantially outperform existing methods like those discussed in, e.g., Cai (2010b), Cai (2010a) and Zhang and Chen (2022), but has not received enough attention. We illustrate this approach and evaluate its performance under models familiar to the psychometric community, including a Multidimensional 2-Parameter Logistic (M2PL) item response theory model and a multilevel logistic regression model with random effects. Secondly, we improve the efficiency of the SOUL algorithm by incorporating a minibatch technique, commonly used in stochastic gradient descent algorithms (Chapter 8.1.3, Goodfellow et al., 2016). The minibatch technique constructs the stochastic gradient using a random subset of the observation units, which can substantially reduce complexity and improve convergence speed for datasets with many observations. As the proposed algorithm involves stochastic sampling in both the sampling and gradient update steps, we call it the Doubly Stochastic Optimisation by Unadjusted Langevin (D-SOUL) algorithm. Simulation studies showed that the proposed algorithm converges substantially faster than the standard SOUL algorithm, while the latter is substantially faster than stochastic optimisation based on the Metropolis-Hastings sampler. Furthermore, the proposed algorithm was applied to estimate an M2PL model for a large-scale personality assessment dataset that involves 30,000 respondents, 300 items, and 30 latent dimensions. Despite the high dimensionality of the model, our algorithm converged successfully within 11 minutes, showing its potential in analysing large-scale data in social and behavioural sciences. The estimation code was written in Julia programming language (Version 1.10.4, Bezanson et al., 2017), and all the code used in this study is available on the Open Science Framework: https://osf.io/3sb4t/?view_only=abd84347053a450fa88f787d168df359.

The rest of the paper is organised as follows. In Section 2, we propose the D-SOUL algorithm under a general latent variable model setting. In Section 3, we establish the theoretical properties of the algorithm, showing that its iterative parameter update converges to the marginal maximum likelihood estimate as the iteration number approaches infinity. We conduct simulation studies in Section 4 to evaluate the performance of the proposed algorithm and compare it with alternative stochastic optimisation algorithms, followed by an application to a large-scale personality assessment dataset in Section 5. We conclude with discussions in Section 6.

2 Proposed Algorithm

2.1 Problem Setup

We consider a latent variable model involving only continuous latent variables. For an observation i , $i = 1, \dots, N$, we let $\mathbf{Y}_i \in \mathbb{R}^{J_i}$ be observed data and $\boldsymbol{\xi}_i \in \mathbb{R}^K$ be the corresponding latent variables. A latent variable model typically assumes that $(\mathbf{Y}_i, \boldsymbol{\xi}_i)$, $i = 1, \dots, N$, are independent, and for each observation i , $(\mathbf{Y}_i, \boldsymbol{\xi}_i)$ is assumed to follow a joint distribution with density function $f_i(\mathbf{y}_i, \boldsymbol{\xi}_i | \boldsymbol{\beta})$, where $\boldsymbol{\beta} \in \mathcal{B} \subset \mathbb{R}^p$ denotes the unknown parameters and \mathcal{B} is the parameter space. The goal is to estimate the unknown parameters $\boldsymbol{\beta}$ by the Marginal Maximum Likelihood Estimator (MMLE), i.e., $\hat{\boldsymbol{\beta}} = \underset{\boldsymbol{\beta} \in \mathcal{B}}{\operatorname{argmax}} l(\boldsymbol{\beta})$, where

$$l(\boldsymbol{\beta}) = \sum_{i=1}^N \log \left(\int f_i(\mathbf{Y}_i, \boldsymbol{\xi}_i | \boldsymbol{\beta}) d\boldsymbol{\xi}_i \right)$$

is the marginal log-likelihood function. We introduce two working examples to make our setting concrete.

Example 1 (Multilevel logistic regression model) *We consider a two-level logistic regression model, following the same setting as in Chapter 12, Bartholomew et al. (2008). Let the level-2 units be indexed by $i = 1, \dots, N$ and the level-1 units be indexed by $j = 1, \dots, J_i$. For level-1 unit j within level-2 unit i , we observe the response variable $Y_{ij} \in \{0, 1\}$. Furthermore, let $\mathbf{x}_{ij} = (x_{ij1}, \dots, x_{ijK})^\top$ be a vector of covariates for level-1 unit j within level-2 unit i , where K is the length of the vector of covariates. Here, x_{ij1} is constrained to be 1 to indicate the random intercept. The level-2 random effects, denoted as $\boldsymbol{\xi}_i = (\xi_{i1}, \dots, \xi_{iK})^\top$ are the latent variables of this model. It is assumed that Y_{i1}, \dots, Y_{iJ_i} are conditionally independent given $\boldsymbol{\xi}_i$, and Y_{ij} given $\boldsymbol{\xi}_i$ follows a Bernoulli distribution satisfying*

$$\mathbb{P}[Y_{ij} = 1 | \boldsymbol{\mu}, \boldsymbol{\xi}_i] = \frac{\exp(\mathbf{x}_{ij}^\top \boldsymbol{\xi}_i)}{1 + \exp(\mathbf{x}_{ij}^\top \boldsymbol{\xi}_i)}.$$

The way \mathbf{x}_{ij} is constrained, ξ_{i1} represents the random intercept term, while $\xi_{i2}, \dots, \xi_{iK}$ represent the random slope terms. The random effects $\boldsymbol{\xi}_i$ are assumed to follow a multivariate normal distribution $\mathcal{N}(\boldsymbol{\mu}, \boldsymbol{\Sigma})$, where $\boldsymbol{\mu} = (\mu_1, \dots, \mu_K)^\top$ is a mean vector and $\boldsymbol{\Sigma}$ is a covariance matrix that is positive-definite. To handle the positive-definite constraint of $\boldsymbol{\Sigma}$, we reparameterise it by Cholesky decomposition, $\boldsymbol{\Sigma} = \mathbf{L}\mathbf{L}^\top$, where $\mathbf{L} = (l_{kk'})_{K \times K}$ is a lower triangular matrix.

To be consistent with our generic notation, we let $\boldsymbol{\beta} = \{\mu_1, \dots, \mu_K, l_{kk'}, k' = 1, \dots, k, k = 1, \dots, K\}$ be all the parameters of the model. As the covariance matrix $\boldsymbol{\Sigma}$ can be expressed as a function of the lower triangular entries of \mathbf{L} , with slight abuse of notation, we denote it as $\boldsymbol{\Sigma}(\boldsymbol{\beta})$. Then $f_i(\mathbf{Y}_i, \boldsymbol{\xi}_i | \boldsymbol{\beta})$

takes the form

$$f_i(\mathbf{Y}_i, \boldsymbol{\xi}_i | \boldsymbol{\beta}) = \left(\prod_{j=1}^{J_i} \frac{\exp(Y_{ij} \mathbf{x}_{ij}^\top \boldsymbol{\xi}_i)}{1 + \exp(\mathbf{x}_{ij}^\top \boldsymbol{\xi}_i)} \right) \phi(\boldsymbol{\xi}_i | \boldsymbol{\mu}, \boldsymbol{\Sigma}(\boldsymbol{\beta})),$$

where $\phi(\boldsymbol{\xi}_i | \boldsymbol{\mu}, \boldsymbol{\Sigma}(\boldsymbol{\beta}))$ is the density function for the multivariate normal distribution $\mathcal{N}(\boldsymbol{\mu}, \boldsymbol{\Sigma}(\boldsymbol{\beta}))$. As no constraint is needed for the parameters in $\boldsymbol{\beta}$, the parameter space $\mathcal{B} = \mathbb{R}^p$, where $p = K + K(K + 1)/2$.

Example 2 (M2PL model) We then consider an M2PL model for confirmatory item factor analysis. In this model, each observation i corresponds to a respondent, and each element of \mathbf{Y}_i records their answer to a binary-scored item. It is assumed that different respondents receive the same set of items, and thus, $J_1 = J_2 = \dots = J_N = J$. The latent variables $\boldsymbol{\xi}_i \in \mathbb{R}^K$ represent unobserved factors measured by the items. The item-factor relationship is characterised by a pre-specified J by K indicator matrix $\mathbf{Q} = (q_{jk})_{J \times K}$, where $q_{jk} = 1$ if factor k is directly measured by item j , and $q_{jk} = 0$ otherwise. Y_{i1}, \dots, Y_{iJ} are assumed to be conditionally independent given $\boldsymbol{\xi}_i$, and Y_{ij} given $\boldsymbol{\xi}_i$ follows a Bernoulli distribution satisfying

$$\mathbb{P}[Y_{ij} = 1 | d_j, \mathbf{a}_j, \boldsymbol{\xi}_i] = \frac{\exp(d_j + \sum_{k=1}^K a_{jk} \xi_{ik})}{1 + \exp(d_j + \sum_{k=1}^K a_{jk} \xi_{ik})},$$

where $a_{jk} = 0$ when $q_{jk} = 0$. The latent variables $\boldsymbol{\xi}_i$ are assumed to follow a multivariate normal distribution $\mathcal{N}(\mathbf{0}, \boldsymbol{\Sigma})$, where the mean vector is constrained to be a zero vector and the diagonal entries of $\boldsymbol{\Sigma}$ are constrained to be one for model identification. Similar to Example 1, we reparameterise $\boldsymbol{\Sigma}$ by $\boldsymbol{\Sigma} = \mathbf{L}\mathbf{L}^\top$, where $\mathbf{L} = (l_{kk'})_{K \times K}$ is a lower triangular matrix satisfying $\sum_{k'=1}^k l_{kk'}^2 = 1$ for all k .

The model parameters $\boldsymbol{\beta} = \{d_1, \dots, d_J\} \cup \{a_{jk} : j = 1, \dots, J, k = 1, \dots, K, q_{jk} = 1\} \cup \{l_{kk'}, k' = 1, \dots, k, k = 1, \dots, K\}$. Similar as Example 1, we express $\boldsymbol{\Sigma}$ as a function of $\boldsymbol{\beta}$, denoted by $\boldsymbol{\Sigma}(\boldsymbol{\beta})$. The joint density function f_i takes the form

$$f_i(\mathbf{Y}_i, \boldsymbol{\xi}_i | \boldsymbol{\beta}) = \left(\prod_{j=1}^J \frac{\exp(Y_{ij} (d_j + \sum_{k=1}^K a_{jk} \xi_{ik}))}{1 + \exp(d_j + \sum_{k=1}^K a_{jk} \xi_{ik})} \right) \phi(\boldsymbol{\xi}_i | \mathbf{0}, \boldsymbol{\Sigma}(\boldsymbol{\beta})).$$

The parameter space $\mathcal{B} = \{\boldsymbol{\beta} \in \mathbb{R}^p : \sum_{k'=1}^k l_{kk'}^2 = 1, k = 1, \dots, K\}$, where $p = J + (\sum_{j=1}^J \sum_{k=1}^K q_{jk}) + K(K + 1)/2$.

2.2 Background on Stochastic Optimisation

A stochastic optimisation algorithm iterates between two steps: (1) sampling the latent variables from their posterior distribution based on the current model parameter estimates, and (2) updating the fixed parameters using an approximate Stochastic Gradient (SG) constructed from the latent variable samples. More precisely, let t be the current iteration number, and let $\beta^{(t-1)}$ and $\xi^{(t-1)}$ be the updated parameters and sampled latent variables in the previous iteration, respectively. The sampling step aims to obtain, for each i , an approximate sample from the posterior distribution of ξ_i given \mathbf{Y}_i evaluated at the model with the parameter $\beta^{(t-1)}$, which is defined as

$$p_{\beta^{(t-1)},i} = \frac{f_i(\mathbf{Y}_i, \xi_i | \beta^{(t-1)})}{\int f_i(\mathbf{Y}_i, \tilde{\xi}_i | \beta^{(t-1)}) d\tilde{\xi}_i}. \quad (1)$$

We also denote the joint posterior of latent variables given \mathbf{Y}_i evaluated at the model with the parameter $\beta^{(t-1)}$ by $\pi_{\beta^{(t-1)}} = \prod_{i=1}^N p_{\beta^{(t-1)},i}$. Typically, exact sampling from the posterior distribution is infeasible. In that case, MCMC methods, such as random walk Metropolis-Hastings (MH) and Gibbs samplers, have been commonly used for generating approximate samples. Such a method uses $\xi_i^{(t-1)}$ as the starting point and samples from a Markov kernel whose invariant distribution is $p_{\beta^{(t-1)},i}$. $\xi_i^{(t)}$ is obtained after one or multiple MCMC iterations.

The parameter update step updates the fixed parameters using an approximate SG. The approximate SG at the t -th iteration takes the form

$$\mathbf{G}_{\beta^{(t-1)}}(\xi^{(t)}) = \sum_{i=1}^N \left(\frac{\partial \log \{f_i(\mathbf{Y}_i, \xi_i^{(t)} | \beta)\}}{\partial \beta} \right) \Big|_{\beta=\beta^{(t-1)}}. \quad (2)$$

We note that if $\xi_i^{(t)}$ is an exact sample from $p_{\beta^{(t-1)},i}$, then $\mathbf{G}_{\beta^{(t-1)}}(\xi^{(t)})$ in (2) is an unbiased estimator of the gradient of the log-marginal-likelihood at $\beta^{(t-1)}$, i.e., $\mathbb{E}_{\pi_{\beta^{(t-1)}}} [\mathbf{G}_{\beta^{(t-1)}}(\xi^{(t)})] = \nabla l(\beta^{(t-1)})$, where the expectation is with respect to $\xi^{(t)}$. As $\xi_i^{(t)}$ obtained from the sampling step is an MCMC approximate sample from $p_{\beta^{(t-1)},i}$, we say $\mathbf{G}_{\beta^{(t-1)}}(\xi^{(t)})$ is an approximate SG evaluated at the t -th iteration. For simplicity, we still call $\mathbf{G}_{\beta^{(t-1)}}(\xi^{(t)})$ an SG when there is no ambiguity. $\beta^{(t)}$ is obtained by an SG ascent step

$$\beta^{(t)} = \beta^{(t-1)} + \gamma_t (\mathbf{D}^{(t)})^{-1} \mathbf{G}_{\beta^{(t-1)}}(\xi^{(t)}), \quad (3)$$

where γ_t is a properly chosen step size that decays to zero as t increases, and $\mathbf{D}^{(t)}$ is a positive definite matrix that is constructed to approximate the second-order information of the marginal log-likelihood. With a constrained parameter space $\mathcal{B} \subset \mathbb{R}^p$, such as in Example 2, a projection is needed in the parameter update step. Instead of (3), [Zhang and Chen \(2022\)](#) suggested to update

β by the quasi-Newton proximal update that solves a projection problem

$$\beta^{(t)} = \underset{\beta \in \mathcal{B}}{\operatorname{argmin}} \|\beta - \beta^{(t-1)} - \gamma_t (\mathbf{D}^{(t)})^{-1} \mathbf{G}_{\beta^{(t-1)}}(\boldsymbol{\xi}^{(t)})\|_{\mathbf{D}^{(t)}}^2, \quad (4)$$

where the norm $\|\cdot\|_{\mathbf{D}^{(t)}}$ is defined as $\|\mathbf{x}\|_{\mathbf{D}^{(t)}}^2 = \mathbf{x}^\top \mathbf{D}^{(t)} \mathbf{x}$. In the special case when $\mathbf{D}^{(t)}$ is constructed to be a diagonal matrix and a well-behaving constrained space \mathcal{B} , (4) can be solved in a closed form. Note that when $\mathcal{B} = \mathbb{R}^p$, then (4) degenerates to the SG ascent update (3).

After completing the two aforementioned steps for a sufficient number of iterations, we obtain a final estimate of β . This estimate can be $\beta^{(t)}$ from the last iteration, or the Polyak-Ruppert trajectory average (Polyak & Juditsky, 1992; Ruppert, 1988) obtained by averaging parameter updates over iterations. Under suitable regularity conditions, these estimates converge to the MMLE $\hat{\beta}$ as the number of iterations grows to infinity, even if $\mathbf{G}_{\beta^{(t-1)}}(\boldsymbol{\xi}^{(t)})$ is only an approximate SG (Atchade et al., 2017; Zhang & Chen, 2022).

Although the existing stochastic optimisation algorithms are substantially faster than many traditional algorithms for high-dimensional models, their computational efficiency can be further improved. Firstly, classical MCMC samplers such as the random walk MH and Gibbs samplers can be very inefficient when the latent dimension K is high (Matthews, 1993; Roberts & Rosenthal, 1998). Additionally, MH samplers typically require tuning (with regard to acceptance rate) to ensure efficient sampling, which can be challenging in practice, especially in a high-dimensional setting. Secondly, the approximate SG in (2) involves a summation over all the N observations, which incurs a high per-iteration cost when N is large. To address these issues, we introduce modifications to improve the computational efficiency of the parameter update and sampling steps.

2.3 Improving Sampling Step: Unadjusted Langevin Sampler

The ULS has been introduced in De Bortoli et al. (2021) for improving the efficiency of the sampling step in stochastic optimisation. Consider sampling from the posterior distribution $p_{\beta^{(t-1)}, i}$ in (1). This ULS is based on a Stochastic Differential Equation (SDE) called the Langevin diffusion

$$d\boldsymbol{\xi}_i(s) = -\nabla U_i(\boldsymbol{\xi}_i(s)) + \sqrt{2}d\mathbf{B}_i(s), \quad s \in [0, \infty),$$

where \mathbf{B}_i is a K -dimensional standard Brownian motion, and U_i is a potential function proportional to the posterior distribution of $\boldsymbol{\xi}_i$. In our setting, the potential function is the negative log-joint density of $(\mathbf{Y}_i, \boldsymbol{\xi}_i)$ given model parameter $\beta^{(t-1)}$ for observation i , which is given as $-\log\{f_i(\mathbf{Y}_i, \boldsymbol{\xi}_i|\beta^{(t-1)})\}$. Under mild assumptions on the negative log-joint density $-\log\{f_i(\mathbf{Y}_i, \boldsymbol{\xi}_i|\beta^{(t-1)})\}$, this SDE has a strong solution for which the posterior distribution of latent variables given the model with parameter $\beta^{(t-1)}$ is the invariant probability measure.

The ULS is an Euler-Maruyama discrete-time approximation to the SDE (Roberts & Tweedie,

1996), as sampling the solution of the SDE is computationally challenging. Compared with traditional MCMC samplers used in stochastic optimisation, such as Metropolis-Hastings (MH) sampler and adaptive rejection Metropolis sampler, the ULS converges faster under high-dimensional settings (Roberts & Tweedie, 1996), by making use of gradient information of the posterior distribution.

We use a ULS update to replace the MCMC sampling update in stochastic optimisation. We denote the gradient of the potential function given the model parameter in the previous iteration $\beta^{(t-1)}$ and evaluated at $\xi_i^{(t-1)}$ as

$$\nabla U_i^{(t-1)} = - \left. \frac{\partial \log \{f_i(\mathbf{Y}_i, \xi_i | \beta^{(t-1)})\}}{\partial \xi_i} \right|_{\xi_i = \xi_i^{(t-1)}}. \quad (5)$$

For example, under the M2PL model, the gradient of the potential function at the t -th iteration is given by

$$\nabla U_i^{(t-1)} = \sum_{j=1}^J \mathbf{a}_j^{(t-1)} \left(\frac{\exp\{d_j^{(t-1)} + (\mathbf{a}_j^{(t-1)})^\top \xi_i^{(t-1)}\}}{1 + \exp\{d_j^{(t-1)} + (\mathbf{a}_j^{(t-1)})^\top \xi_i^{(t-1)}\}} - Y_{ij} \right) + \{\Sigma(\beta^{(t-1)})\}^{-1} \xi_i^{(t-1)},$$

where $a_{jk} = 0$ when $q_{jk} = 0$. Then, we obtain $\xi_i^{(t)}$ by

$$\xi_i^{(t)} = \xi_i^{(t-1)} - h_t \nabla U_i^{(t-1)} + \sqrt{2h_t} \mathbf{Z}_i^{(t)},$$

where h_t is the Euler-Maruyama discretisation step size that decays to zero as t increases, and $\mathbf{Z}_i^{(t)}$ is a white noise vector following a K -dimensional standard normal distribution. The specific choice of h_t is given in Section 3, which is guided by the convergence theory of the algorithm.

2.4 Proposed D-SOUL Algorithm

We improve the efficiency of the parameter update step by applying a minibatch technique when constructing the SG. In the standard SG update (2), the summation is over all the observation units, which can be computationally expensive when the number of observation units is very large. As an alternative, we consider a minibatch SG. In the t -th iteration, we randomly draw a subset of $\{1, \dots, N\}$ of size n , denoted by $S^{(t)}$. Then, we construct the minibatch SG as:

$$\mathbf{G}_{\beta^{(t-1)}}^{\text{mini}}(\xi^{(t)}, S^{(t)}) = \frac{N}{n} \sum_{i=1}^N \mathbb{1}_{\{i \in S^{(t)}\}} \left(\frac{\partial \log \{f_i(\mathbf{Y}_i, \xi_i^{(t)} | \beta)\}}{\partial \beta} \right) \Bigg|_{\beta = \beta^{(t-1)}}. \quad (6)$$

It is easy to see that when $\xi_i^{(t)}$ is an exact sample from $p_{\beta^{(t-1)}, i}$ for all i , $\mathbf{G}_{\beta^{(t-1)}}^{\text{mini}}(\xi^{(t)}, S^{(t)})$ is a stochastic gradient of the marginal likelihood at $\beta^{(t-1)}$. By choosing n to be much smaller than

N , one can substantially reduce the per-iteration computational complexity, as the summation in (6) reduces to n terms. It also means that instead of sampling all the $\xi_i^{(t)}$ in the sampling step, one only needs to sample all the $\xi_i^{(t)}$ within the minibatch $S^{(t)}$. Compared with the standard SG, an algorithm using the minibatch SG tends to converge faster. That is because, with the same computation budget (in terms of processed observation units) for one standard SG update, the minibatch SG has already updated the parameters N/n times.

When implementing the minibatch SG update, an important decision to make is the minibatch size n . Theoretically, one should set $n = 1$, as it leads to the fastest convergence speed because it updates the parameters most frequently when processing the same number of observation units. However, the implementation of minibatch SG update with $n = 1$ is not particularly computationally efficient since CPUs and GPUs cannot exploit the full power of vectorisation (Chapter 12.5, Zhang et al., 2024). Choosing a minibatch size between 1 and N achieves a trade-off between the statistical convergence speed (regarding the number of observation units processed) and computational efficiency (regarding the average CPU/GPU processing time per sample). We consider three minibatch sizes ($n = 10, 50, 100$) in the simulation study. Its results show that the minibatch size of $n = 50, 100$ attains fast convergence robustly under all the simulation conditions, although that of $n = 10$ presents slower convergence than the other minibatch sizes in a complex model setting. Thus, a smaller minibatch size does not necessarily provide a suitable one for actual implementations because of the trade-off between the statistical convergence speed and computational efficiency.

The proposed D-SOUL algorithm incorporates the minibatch gradient update into the ULS-based SOUL algorithm. It is summarised in Algorithm 1 below. We provide a few remarks regarding the implementation of this algorithm. First, we do not give a specific stopping criterion here. Due to the randomness in both algorithm steps, we believe that a stopping criterion based on parameter change in a small number of consecutive iterations does not perform well. We suggest making the stopping decision by monitoring the trace plot for the trajectories of all the model parameters. Specifically, we stop the algorithm when all the parameters are stable, i.e., each fluctuating around a stable level.

Second, there is freedom regarding the construction of $\mathbf{D}^{(t)}$. In our implementation, we set $\mathbf{D}^{(t)}$ to be a diagonal matrix that does not change over iterations, where the diagonal entries differ for different parameters for better scaling the corresponding gradients. An advantage of choosing $\mathbf{D}^{(t)}$ to be diagonal is that the quasi-Newton proximal update has a closed-form solution, which is important in estimating the M2PL model. Alternatively, one can update $\mathbf{D}^{(t)}$ adaptively during the iterations, following the methods considered in Zhang and Chen (2022) and Cai (2010a). We do not consider these choices of $\mathbf{D}^{(t)}$ to keep the focus of this article on the advantages brought by the ULS and minibatch gradient.

Finally, we note that a common issue with stochastic optimisation is the sensitivity of the

algorithm’s empirical convergence to the choice of step sizes (Asi & Duchi, 2019). Slow convergence can occur if the step sizes decay too quickly. To address this, we introduce an initialisation stage that involves a sufficient number of iterations of Algorithm 1. During this stage, the parameters h_t and γ_t are set as constants that do not decay with t . This stage can provide reasonably accurate, while slightly biased, estimates of $\beta^{(t)}$ and $\xi^{(t)}$, which will be refined by further iterations of Algorithm 1 with decaying h_t and γ_t . As shown in Section 3, when h_t and γ_t decay at appropriate rates, $\beta^{(t)}$ will converge to the MMLE as t goes to infinity.

Algorithm 1: D-SOUL Algorithm

Input: Minibatch size n , the initial values of model parameter $\beta^{(0)}$ and latent variables $\xi^{(0)}$, and step sizes $h_1, \gamma_1, h_2, \gamma_2, \dots$

for iterations $t = 1, 2, \dots$, **do**

1. Sample minibatch $S^{(t)} \subset \{1, \dots, N\}$.
2. For all $i \in S^{(t)}$, sample $\mathbf{Z}_i^{(t)}$ from K -variate standard normal distribution and update $\xi_i^{(t)}$ by

$$\xi_i^{(t)} = \xi_i^{(t-1)} - h_t \nabla U_i^{(t-1)} + \sqrt{2h_t} \mathbf{Z}_i^{(t)},$$

where $\nabla U_i^{(t-1)}$ is computed by (5). For $i \notin S^{(t)}$, $\xi_i^{(t)} = \xi_i^{(t-1)}$.

3. Update $\mathbf{D}^{(t)}$, if necessary.
4. Construct the minibatch SG

$$\mathbf{G}_{\beta^{(t-1)}}^{\text{mini}}(\xi^{(t)}, S^{(t)}) = \frac{N}{n} \sum_{i=1}^N \mathbb{1}_{\{i \in S^{(t)}\}} \left(\frac{\partial \log \{f_i(\mathbf{Y}_i, \xi_i^{(t)} | \beta)\}}{\partial \beta} \right) \Bigg|_{\beta = \beta^{(t-1)}}.$$

5. Update the model parameter by minibatch SG update

$$\beta^{(t)} = \beta^{(t-1)} + \gamma_t (\mathbf{D}^{(t)})^{-1} \mathbf{G}_{\beta^{(t-1)}}^{\text{mini}}(\xi^{(t)}, S^{(t)})$$

when the parameter space is unconstrained, and by minibatch quasi-Newton proximal update

$$\beta^{(t)} = \operatorname{argmin}_{\beta \in \mathcal{B}} \|\beta - \beta^{(t-1)} - \gamma_t (\mathbf{D}^{(t)})^{-1} \mathbf{G}_{\beta^{(t-1)}}^{\text{mini}}(\xi^{(t)}, S^{(t)})\|_{\mathbf{D}^{(t)}}^2.$$

until stopping decision is met. Let T be the final iteration number.

Output: $\hat{\beta} = \beta^{(T)}$.

3 Theoretical Convergence

In what follows, we provide the convergence guarantee for the proposed algorithm. It extends Theorem 5 in [De Bortoli et al. \(2021\)](#) to the setting where the SG is constructed using minibatches. The proof of this theorem is given in the Supplementary Materials [A.1](#).

Theorem 1 *Assume Assumptions 1-6 (see the Supplementary Materials [A.1](#)) hold, $-l(\beta)$ is convex, $\mathbf{D}^{(t)}$ is set to be an identity matrix, and \mathcal{B} is compact and convex. For sufficiently large t , choose $\gamma_t = \mu_1 t^{-a}$ and $h_t = \mu_2 t^{-b}$, such that $\gamma_1 < 1/L_1$, $h_1 < \bar{h}$ with $\bar{h} > 0$, $a \leq 1$, $a + b/2 > 1$, $2a - 2b > 1$, $a + (b + 1) - 3b > 1$, and μ_1 and μ_2 are any positive constants, where L_1 is the Lipschitz constant in Assumption 2.*

Then, $(\beta^{(t)})_{t \in \mathbb{N}}$ from the D-SOUL algorithm converges a.s to some $\hat{\beta} \in \underset{\beta \in \mathcal{B}}{\operatorname{argmax}} l(\beta)$.

We provide a few remarks about this theoretical result. First, we note that the theorem provides guidance on choosing step sizes for the ULS and the minibatch SG steps. In the actual implementation, we set $a = 0.84$ and $b = 0.33$, to ensure that the step sizes do not decay too fast while still guaranteeing convergence.

Second, the theorem assumes that the negative marginal log-likelihood function is convex. However, this assumption does not hold for most latent variable models, including the two examples considered in this paper. It is possible to relax this assumption to allow $-l(\beta)$ to be nonconvex, following a similar proving strategy as Theorem S19 of [De Bortoli et al. \(2021\)](#). But in that case, we can only show that $\beta^{(t)}$ converges to a stationary point of $l(\beta)$ that is not necessarily an MMLE. Nevertheless, our simulation studies show that the algorithm has good empirical convergence behaviour. Using random starting points, the D-SOUL algorithm always converges to solutions that are close to the true model parameters under the two models we have considered.

Third, Theorem 1 assumes that $\mathbf{D}^{(t)}$ is an identity matrix. Similar to [Zhang and Chen \(2022\)](#), this assumption can be relaxed by requiring $\mathbf{D}^{(t)}$ to be positive definite with its maximum and minimum eigenvalues to be bounded above and below, respectively.

Fourth, in Theorem 1, it is assumed that \mathcal{B} is compact and convex for the almost sure convergence of $\beta^{(t)}$ to $\hat{\beta} \in \underset{\beta \in \mathcal{B}}{\operatorname{argmax}} l(\beta)$, which can be guaranteed by the quasi-Newton proximal update with $\mathbf{D}^{(t)}$ being an identity matrix. However, this assumption is made for the theoretical convergence of $\beta^{(t)}$ rather than the actual implementation of the D-SOUL algorithm that ensures the convergence. Thus, in practice, we do not apply the quasi-Newton proximal update unless there is a specific parameter constraint, such as in the correlation matrix of the M2PL model. Instead, we update the model parameter by a minibatch SG update, which corresponds to the quasi-Newton proximal update in (4) under $\mathcal{B} = \mathbb{R}^p$, as illustrated in Algorithm 1. This is because a set of the possible values that can be taken in numerical computations is bounded and convex, except for the numerically unstable case of values taking ∞ .

Lastly, Theorem 1 can be further extended following the theoretical developments in Zhang and Chen (2022) to provide a theoretical guarantee for the constrained optimisation based on (4) including the setting where the objective function contains a non-smooth function. With additional regularity conditions on the constrained space \mathcal{B} and a non-smooth function, one can show that $\beta^{(t)}$ converges to a stationary point of the constrained optimisation problem.

4 Simulation Study

We compare the proposed D-SOUL algorithm with two other algorithms using simulations. The first algorithm is the SOUL algorithm, which can be seen as a special case of the D-SOUL algorithm with batch size $n = N$. The second algorithm is stochastic optimisation denoted by the SOMH, which replaces the ULS in the SOUL algorithm with a random walk MH sampler. The purpose of this comparison is three-fold:

1. By comparing the SOUL and SOMH algorithms, we hope to show that the ULS makes the stochastic optimisation algorithm converge faster, especially when the latent dimension K is high.
2. By comparing the SOUL algorithm and the D-SOUL algorithm with different minibatch sizes, we aim to show the effectiveness of using minibatch gradients. This will help show the tradeoff between statistical convergence speed and computational efficiency when choosing the minibatch size.
3. Show the effectiveness of the D-SOUL algorithm in estimating the two latent variable models we have considered.

The simulations are conducted using the multilevel logistic regression and M2PL models.

4.1 Simulation Settings

The following simulation settings are considered for the multilevel logistic regression and M2PL models.

Multilevel logistic regression model. In the multilevel logistic regression model, we explore two different scenarios: a lower-dimensional setting and a higher-dimensional setting. In the lower-dimensional setting, there are 10,000 level-2 units ($N = 10,000$), with ten level-1 units observed within each level-2 unit ($J_i = 10$). We set the number of covariates to $K = 3$, including the value of 1 to denote a random intercept resulting in three latent variables. In the higher-dimensional setting, there are 10,000 level-2 units ($N = 10,000$), with twenty level-1 units observed within

each level-2 unit ($J_i = 20$). The number of covariates is set to $K = 10$, resulting in ten latent variables.

In both settings, the values of covariates were generated from a multivariate normal distribution with the zero vector $\mathbf{0}_{K-1}$ and a correlation matrix with diagonal and off-diagonal elements set to 1.0 and 0.5, respectively. For the fixed effects of the model, the true intercept was set to 0.3, and the true slopes were generated from $\text{Uniform}(0, 1)$. The true values of these fixed effects are given in Supplementary Materials A.2.1. The diagonal and off-diagonal elements of the covariance matrix Σ of the random effects were set to 0.1 and 0.05, respectively. Lastly, one hundred datasets were simulated under each setting to compare the stochastic optimisation algorithms.

M2PL model. Under the confirmatory M2PL model, we consider both lower- and higher-dimensional settings. In the lower-dimensional setting, we set the number of respondents and items to $N = 10,000$ and $J = 50$, while the number of latent variables was set to $K = 3$. In the higher-dimensional setting, we set the number of respondents and items to $N = 10,000$ and $J = 200$, and the number of latent variables was set to $K = 10$.

In both settings, the diagonal and off-diagonal elements of the latent variables correlation matrix Σ were set to 1.0 and 0.5, respectively. The indicator matrix \mathbf{Q} in the lower-dimensional setting was specified to include all the possible patterns of a row vector of \mathbf{Q} (i.e., $\mathbf{q}_1 = (1, 0, 0)$, $\mathbf{q}_2 = (0, 1, 0)$, \dots , $\mathbf{q}_6 = (0, 1, 1)$, $\mathbf{q}_7 = (1, 1, 1)$) and concatenate seven sets of these possible patterns with $\mathbf{q}_7 = (1, 1, 1)$. That in the higher-dimensional setting was specified to include two identity matrices, a set of all the possible row-vector patterns such that two or three out of ten latent variables are directly measured, and randomly chosen 15 possible row-vector patterns such that two, three, or three out of ten latent variables are directly measured. The intercept parameter d_j values were generated from a standard normal distribution, while the non-zero factor loading parameter a_{jk} values were generated from a uniform distribution in the interval (0.5, 1.5). Due to space constraints, specific values of these item parameters are not given in the Supplementary Materials; however, the values are available on the Open Science Framework: https://osf.io/3sb4t/?view_only=abd84347053a450fa88f787d168df359. The latent variables were generated from a multivariate normal distribution $\mathcal{N}(\mathbf{0}_K, \Sigma)$. Lastly, one hundred artificial datasets were generated under each setting.

We consider different minibatch sizes for the D-SOUL algorithm, including $n = 10, 50$, and 100. Additionally, we fix the implementation details to ensure a relatively fair comparison between the algorithms as follows:

1. All the algorithms start with the same initial values for model parameters and latent variables, $\beta^{(0)}$ and $\xi^{(0)}$. These initial values are obtained by making a small perturbation to the true parameter values and latent variables; see Supplementary Materials A.2.2 for the details. We adopted this approach as different algorithms may have different levels of sensitivity of the

starting point, and it minimises the impact of such a sensitivity on the performance of the algorithms.

2. We do not use a constant step-size initialisation stage for all the algorithms, as a good starting point is already employed. For the D-SOUL and SOUL algorithms, we set the step sizes $\gamma_t = \mu_1 t^{-0.84}$ and $h_t = \mu_2 t^{-0.33}$, where μ_1 and μ_2 are chosen from a set of 5 candidate values. Details can be found in the Supplementary Materials [A.2.3](#). The SOMH algorithm does not involve h_t , so we set $\gamma_t = \mu_1 t^{-0.84}$ and choose μ_1 from its candidate set. In addition, we choose the random walk step size from 5 candidate values. As the minibatch SG updates the parameters N/n times using the same computational budget (in terms of processed observation units) for one standard SG update, we let γ_t and h_t decay after N/n model parameter updates in the D-SOUL algorithm. With this decaying schedule, the step sizes decay at a similar rate for all algorithms in terms of processed observation units. This means that after processing N observation units in model parameter updates, the step sizes for all the algorithms will decay. For each algorithm, we present the best result among those given by different tuning parameters. We also discuss how sensitive the algorithms are to the choice of tuning parameters.
3. Regarding the choice of $\mathbf{D}^{(t)}$, the diagonal elements of $\mathbf{D}^{(t)}$ corresponding to the Cholesky-decomposed part of a covariance/correlation matrix, \mathbf{L} , were prespecified to rescale the corresponding step sizes by 1/500 in all the algorithms for numerical stability. We have tried different scaling values, and this specification prevents the gradient of \mathbf{L} from divergence and stabilises parameter learning in all the simulation conditions. The diagonal elements of $\mathbf{D}^{(t)}$ corresponding to the other parameters were prespecified to the identity matrix, meaning that no rescaling was applied to them.

4.2 Evaluation Criteria

To evaluate the convergence speed of the algorithms, we use a similar evaluation scheme as in Zhang et al. (Chapter 12.5; 2024). In particular, we save the values of updated model parameters every 0.005 seconds during the iterations until the elapsed time in updating model parameters reaches 3 seconds. After that, we compute the error using the saved updated parameter values and create an error trajectory as a function of the elapsed time.

In addition, we evaluated the error of model parameters using the mean absolute error (MAE). We stored and utilised the model parameters updated at a specific time point, denoted by \tilde{t} , to compute the error. Our specific time points ranged from $\tilde{t} = 0.005, 0.01, \dots, 3.0$. In the multilevel logistic regression model, we computed the absolute errors (AE) of the mean vector of random effects $\boldsymbol{\mu}$ and the covariance matrix $\boldsymbol{\Sigma} = (\sigma_{kk'})_{K \times K}$ reparametrised by \mathbf{L} at the \tilde{t} -th time point in

the r -th simulated dataset given by

$$\begin{aligned}\text{AE}_{\boldsymbol{\mu}}^{(\tilde{t}), (r)} &= \frac{1}{K} \sum_{k=1}^J \left| \mu_k^{(\tilde{t}), (r)} - \mu_k^* \right| \\ \text{AE}_{\boldsymbol{\Sigma}}^{(\tilde{t}), (r)} &= \frac{1}{K^2} \sum_{k=1}^J \sum_{k'=1}^J \left| \sigma_{kk'}^{(\tilde{t}), (r)} - \sigma_{kk'}^* \right|,\end{aligned}$$

where the parameter with superscript $*$ denotes its true value, and the parameter with superscript $(\tilde{t}), (r)$ denotes its updated value at the \tilde{t} -th time point in the r -th simulated dataset. Then, the MAE for the multilevel logistic regression model at the \tilde{t} -th time point was computed as

$$\text{MAE}_{\text{Multilevel}}^{(\tilde{t})} = \frac{1}{100} \sum_{r=1}^{100} \frac{1}{2} \left(\text{AE}_{\boldsymbol{\mu}}^{(\tilde{t}), (r)} + \text{AE}_{\boldsymbol{\Sigma}}^{(\tilde{t}), (r)} \right), \quad (7)$$

where 100 is the number of simulated datasets in the simulation study. The MAEs of each model parameter were also computed in the same manner as (7).

In the confirmatory M2PL model, the AEs of the intercept parameter d_1, \dots, d_J , factor loading parameter $\mathbf{a}_1, \dots, \mathbf{a}_J$, and the correlation matrix $\boldsymbol{\Sigma} = (\sigma_{kk'})_{K \times K}$ reparametrised by \mathbf{L} at the \tilde{t} -th time point in the r -th simulated dataset were computed as

$$\begin{aligned}\text{AE}_{d_1, \dots, d_J}^{(\tilde{t}), (r)} &= \frac{1}{J} \sum_{j=1}^J \left| d_j^{(\tilde{t}), (r)} - d_j^* \right| \\ \text{AE}_{\mathbf{a}_1, \dots, \mathbf{a}_J}^{(\tilde{t}), (r)} &= \frac{1}{\sum_{j=1}^J \sum_{k=1}^K q_{jk}} \sum_{j=1}^J \sum_{k=1}^K q_{jk} \left| a_{jk}^{(\tilde{t}), (r)} - a_{jk}^* \right| \\ \text{AE}_{\boldsymbol{\Sigma}}^{(\tilde{t}), (r)} &= \frac{1}{K^2} \sum_{k=1}^J \sum_{k'=1}^J \left| \sigma_{kk'}^{(\tilde{t}), (r)} - \sigma_{kk'}^* \right|.\end{aligned}$$

Subsequently, the MAE for the confirmatory M2PL model at the \tilde{t} -th time point was computed as

$$\text{MAE}_{\text{M2PL}}^{(\tilde{t})} = \frac{1}{100} \sum_{r=1}^{100} \frac{1}{3} \left(\text{AE}_{d_1, \dots, d_J}^{(\tilde{t}), (r)} + \text{AE}_{\mathbf{a}_1, \dots, \mathbf{a}_J}^{(\tilde{t}), (r)} + \text{AE}_{\boldsymbol{\Sigma}}^{(\tilde{t}), (r)} \right). \quad (8)$$

The MAEs of each model parameter were also computed in the same manner as (8).

Due to space limitations, we present the average trajectories of the MAEs as given in (7) and (8). The trajectories of the MAE for each parameter are given in the Supplementary Materials A.3.

4.3 Results from Multilevel Logistic Regression Model

We present the results for the multilevel logistic regression model. Figures 1 and 2 show the error trajectories of $\text{MAE}_{\text{Multilevel}}^{(\tilde{t})}$ for the settings with $K = 3, 10$. Note that since we computed the error of updated model parameters every 0.005 seconds, some trajectories in the figures have a horizontal

line at the beginning. This horizontal part means that the first model parameter update was not completed, and the error based on the initial values is presented during the corresponding time period.

First, we compare the SOUL and SOMH algorithms. Figures 1 and 2 show that the errors of the SOUL algorithm were consistently lower than those of the SOMH algorithm at all time points. There are two reasons for this. First, the MH algorithm requires an accept-reject step in the posterior sampling of latent variables, which involves computing the complete-data log-likelihood for the previously sampled and proposed latent variables. This step requires processing $2J$ level-1 units for the accept-reject step for observation i , doubling the computational budget compared to the SOUL algorithm, which requires processing J level-1 units to compute a gradient for observation i . Thus, the SOMH algorithm updates a model parameter less frequently than the SOUL algorithm within the same time window. The second reason is that the SOMH algorithm does not take advantage of the geometric information of a potential function (i.e., the gradient of the negative complete-data log-likelihood) to sample a proposed value of latent variables, which makes it less efficient as the dimension of the latent variable increases. This leads to less accurate sampling of the latent variables compared to the SOUL algorithm, and the standard SG becomes less accurate in approximating the true gradient (i.e., the gradient of a marginal likelihood). On the other hand, the unadjusted Langevin sampler utilises the geometric information, resulting in better performance in high dimensional settings and more efficient sampling of the latent variables to approximate the true gradient.

Second, we compare the D-SOUL algorithm with the minibatch size of $n = 10, 50, 100$ and the SOUL algorithm. In both the lower- and higher-dimensional settings, the errors of the D-SOUL algorithm with $n = 10, 50, 100$ were consistently lower than those of the SOUL algorithm, showing the faster convergence of the D-SOUL algorithm. This result was obtained because the D-SOUL algorithm could update model parameters more frequently than the SOUL algorithm within the same computational budget for one standard SG update of the SOUL algorithm. Regarding the comparison among the different minibatch sizes, all the D-SOUL algorithms showed similar behaviour in the lower-dimensional setting. In the higher-dimensional setting, while the D-SOUL algorithm with $n = 10$ reduced the error most initially, all the D-SOUL algorithms converged to the same magnitude of the MAE after three seconds. Thus, the behaviors of the D-SOUL algorithm with the different minibatch sizes were generally similar in this model setting.

Overall, the findings from this simulation show that the D-SOUL algorithm achieves faster convergence with more accurate model parameters than the other competitors within the given time frame.

Multilevel logistic regression model with $K=3$

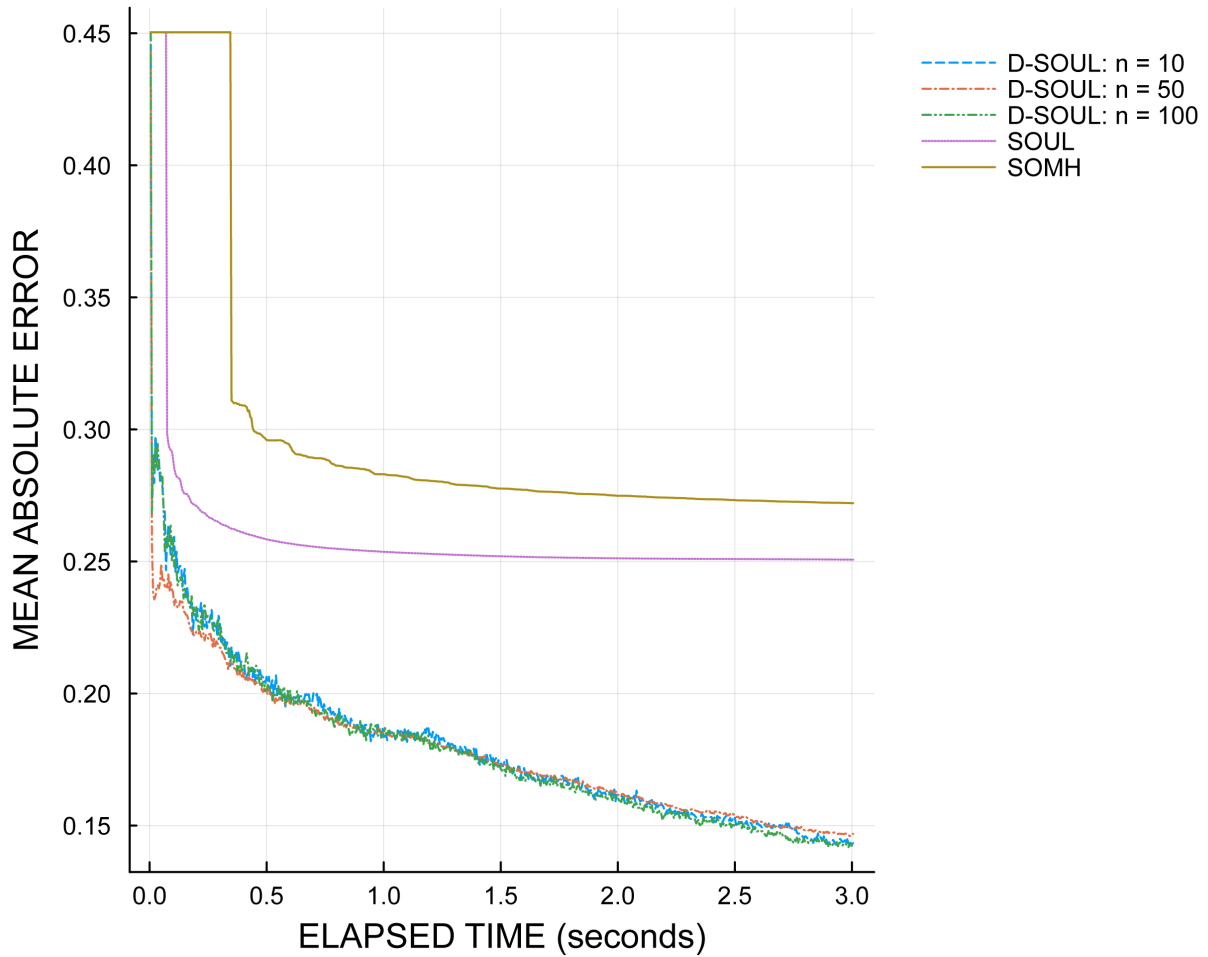


Figure 1: The trajectory of the MAE as a function of elapsed time: the multilevel logistic regression model with $K = 3$. The blue-dash, red-dashdot, green-dashdotdot, purple-dot, and brown-solid lines denote the trajectories from the D-SOUL algorithms with $n = 10, 50, 100$, SOUL, and SOMH algorithms, respectively.

Multilevel logistic regression model with $K=10$

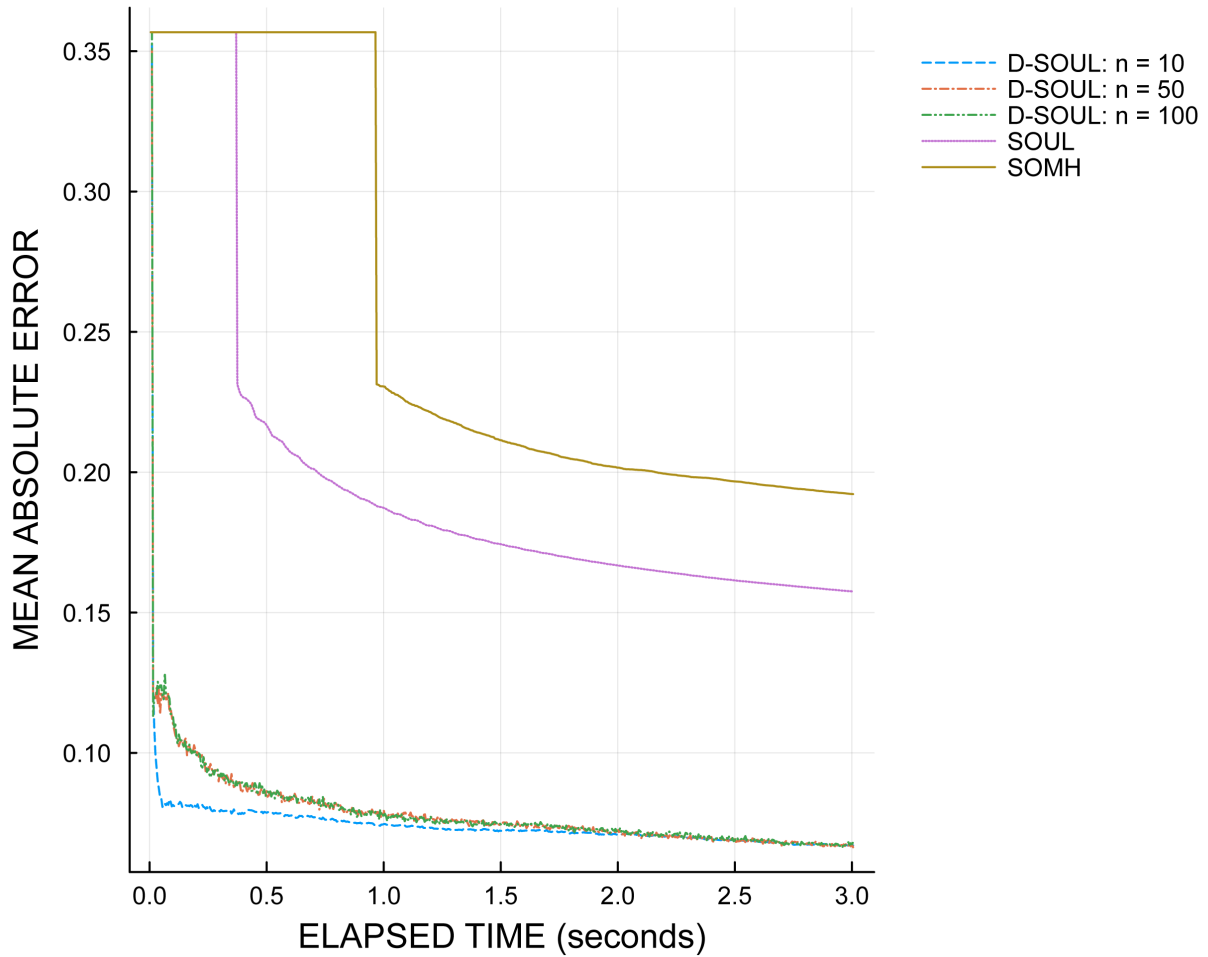


Figure 2: The trajectory of the MAE as a function of elapsed time: the multilevel logistic regression model with $K = 10$. The blue-dash, red-dashdot, green-dashdotdot, purple-dot, and brown-solid lines denote the trajectories from the D-SOUL algorithms with $n = 10, 50, 100$, SOUL, and SOHM algorithms, respectively.

4.4 Results from M2PL Model

Next, we will present the results of the confirmatory M2PL model. Figures 3 and 4 display the error trajectories of $\text{MAE}_{\text{M2PL}}^{(i)}$ under the settings with $K = 3, 10$.

Similar to the results from the multilevel logistic regression model, the SOUL algorithm consistently exhibited lower errors compared to the SOMH algorithm across all time points. Additionally, the gap between these two algorithms becomes larger under $K = 10$ than $K = 3$. These findings suggest that the SOUL algorithm scales better with an increase in the number of latent variables and achieves faster convergence than the SOMH algorithm.

The comparison between the D-SOUL algorithm with minibatch size of $n = 10, 50, 100$ and the SOUL algorithm shows that the D-SOUL algorithm consistently has lower errors than the SOUL algorithm in both lower- and higher-dimensional settings. The D-SOUL algorithm updates model parameters more frequently than the SOUL algorithm within the same computational budget for one standard SG update of the SOUL algorithm. Thus, the D-SOUL results in faster convergence.

When comparing different minibatch sizes, the D-SOUL algorithm with $n = 50, 100$ behaved similarly while the algorithm with $n = 10$ performed worse across all time points. The poor performance of the D-SOUL algorithm with $n = 10$ is due to the trade-off between statistical convergence and computational efficiency. A smaller minibatch size leads to more frequent model parameter updates but also reduces computational efficiency in terms of the average CPU/GPU processing time per sample due to each model parameter update requiring computing matrix-vector multiplications and sampling observations in a minibatch. On the other hand, a larger minibatch leads to fewer parameter updates, which means that the statistical efficiency in terms of the number of observation units processed for convergence decreases. However, as a larger minibatch involves fewer parameter updates, the computational efficiency is not reduced to the extent that a smaller minibatch does. Accordingly, this result suggests that using a relatively large minibatch size, such as $n = 50, 100$, can be the best option in terms of both statistical convergence speed and computational efficiency. Overall, our simulation illustrates the fast convergence of the D-SOUL algorithm.

5 Application to International Personality Item Pool NEO personality inventory

In this section, we will be using the D-SOUL algorithm to fit the confirmatory M2PL model to personality assessment data obtained from the International Personality Item Pool – Neuroticism, Extraversion, and Openness (IPIP-NEO) personality inventory (Johnson, 2014). Our focus will be on examining the relationship between the measurement items and their corresponding personality traits, as well as on the correlation structure of these latent traits.

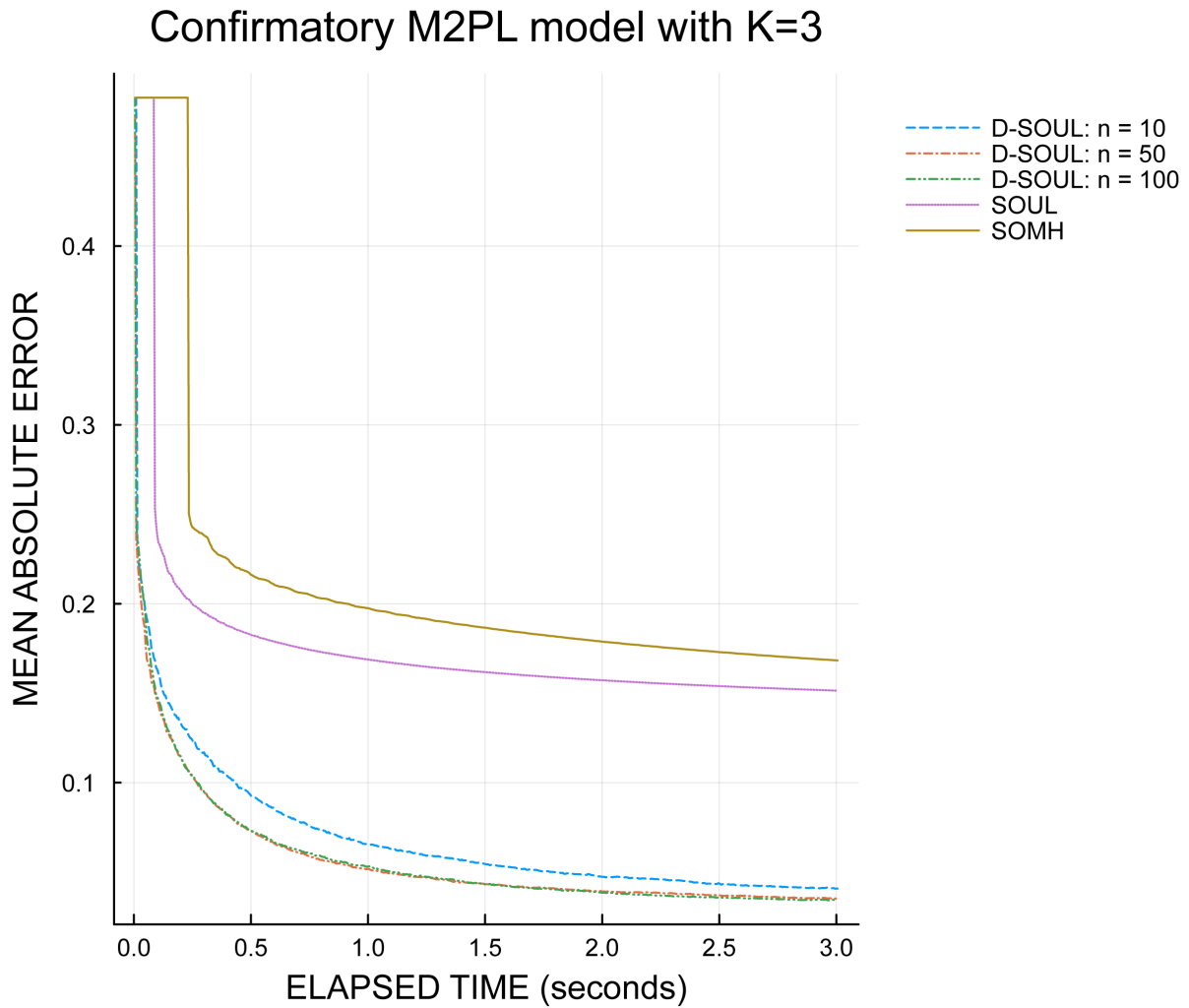


Figure 3: The trajectory of the MAE as a function of elapsed time: the confirmatory M2PL model with $K = 3$. The blue-dash, red-dashdot, green-dashdotdot, purple-dot, and brown-solid lines denote the trajectories from the D-SOUL algorithms with $n = 10, 50, 100$, SOUL, and SOHM algorithms, respectively.

Confirmatory M2PL model with $K=10$

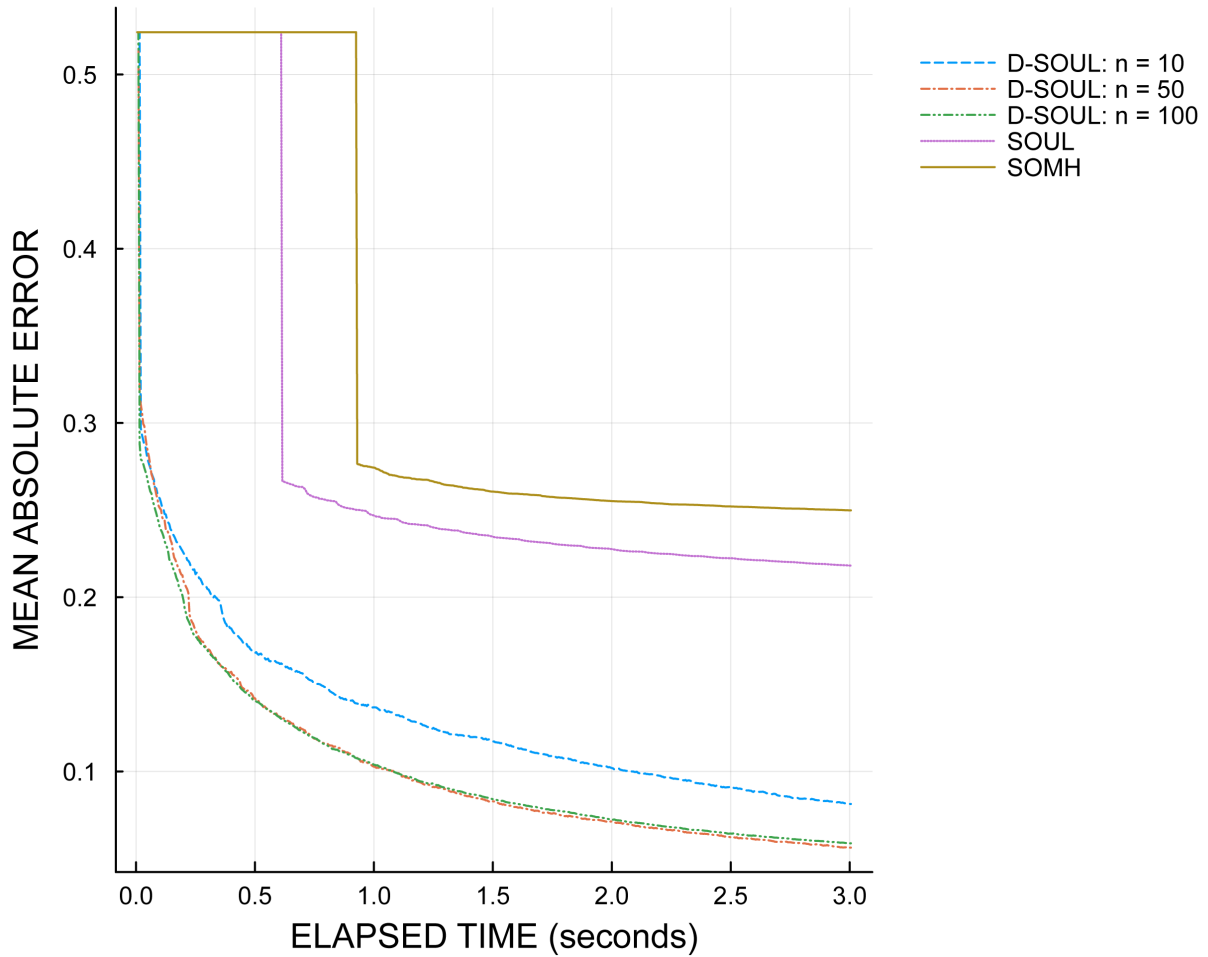


Figure 4: Trajectory of the MAEs a function of elapsed time: confirmatory M2PL model with $K = 10$. The blue-dash, red-dashdot, green-dashdotdot, purple-dot, and brown-solid lines denote the trajectories from the D-SOUL algorithms with $n = 10, 50, 100$, SOUL, and SOHM algorithms, respectively.

5.1 Data Description

The dataset used in this study was obtained from the repository of [Johnson \(2014\)](#) on the Open Science Framework: <https://osf.io/wxvth/>. It includes 307,313 cases of item responses to the IPIP-NEO-300 inventory, which measured the big five personality traits: openness to experience (O), conscientiousness (C), extraversion (E), agreeableness (A), and neuroticism (N). According to [Johnson \(2014\)](#), each personality trait consists of six facets, resulting in 30 personality traits for the inventory. For example, openness to experience consists of the following six facets: Imagination (O1), Artistic interests (O2), Emotionality (O3), Adventurousness (O4), Intellect (O5) and Liberalism (O6). Each facet is measured by ten items, making the total number of items 300. For this empirical illustration, a randomly chosen subset of 30,000 cases was used, where each case completed all 300 items. The items were originally measured on a five-point Likert-scale. In the analysis, the items were dichotomised by computing the median of each item and coding an item response equal to or larger than the median of the corresponding item to the value of 1, and 0 otherwise.

5.2 Estimation Settings

We applied the confirmatory M2PL model to this dataset and utilised the D-SOUL algorithm for parameter estimation. The specifications for the parameter estimation are as follows.

In the initialisation stage for obtaining good starting values, we ran the D-SOUL algorithm with $n = 50$ using fixed step sizes of $\gamma_t = 5.0$ and $h_t = 0.01$ for 150 data passes. The number of data passes is the cumulative number of observations used to construct a minibatch SG, divided by n . The 150 data passes imply running the algorithm until the number of observations used to construct a minibatch SG during the iterations reaches $150N$. Regarding the initial values in the initialisation stage, the latent variables were set to the standardised observed sum scores computed on the items that measure the same factor. The initial values of intercept parameters were set to zero, while those of non-zero factor loading parameters were set to 1. The initial value of the correlation matrix was based on the correlations computed from the initial values of latent variables. The updated model parameters at the last iteration were then used as the starting point for a subsequent analysis.

After obtaining the starting values in the initialisation stage, we used the D-SOUL algorithm with $n = 50$ and employed decaying step sizes of $\gamma_t = 5.0 \times t^{-0.84}$ and $h_t = 0.01 \times t^{-0.33}$ for 250 data passes. These step sizes satisfy the step-size conditions in Theorem 1. Similar to the simulation study, we let γ_t and h_t decay after every N/n model parameter updates. We determined the number of data passes from the trace plot of the updated model parameters (see A4 in the Supplementary Materials). The final estimates were obtained from the updated model parameters at the last iteration.

Note that the total number of data passes is 400, which may seem like a large number of iterations. However, this number of data passes was chosen to accommodate the two unexpectedly large factor loading parameters, which require a large number of iterations to achieve convergence.

Lastly, for numerical stability, we set $\mathbf{D}^{(t)}$ to rescale the step size for updating the Cholesky-decomposed part of a correlation matrix, \mathbf{L} , by 1/500. For the other model parameters, we set the corresponding diagonal elements of $\mathbf{D}^{(t)}$ to the identity matrix. This specification was applied both during the initialisation and subsequent stages.

5.3 Results

The estimated factor loadings and latent factor correlation matrix are given in Table 1 and Figure 5, respectively. In Table 1, only the non-zero factor loadings corresponding to the indicator matrix \mathbf{Q} are shown. The indicator matrix \mathbf{Q} is set to have a simple structure where each item measures only one factor, and each factor is measured by ten items. The values in the ten columns under “Factor Loading Parameters” present the factor loadings of each item related to the relevant latent trait.

Our analysis revealed similar patterns to a previous study that examined the same personality inventory (Zhang et al., 2020). It should be noted that the dataset in our study is different from the one used in the previous study, which utilised a sample size of 7,325 from Johnson (2005). In contrast, the dataset used in this study is adopted from Johnson (2014). All the estimated factor loading in Table 1 are positive, and consistent with the results reported in Zhang et al. (2020).

Additionally, Figure 5 shows that the correlation matrix contains large positive correlation coefficients in the diagonal blocks formed by facets belonging to the same personality trait. This finding aligns with the design of the personality inventory and is consistent with the previous study (Zhang et al., 2020). Furthermore, the correlations between the facets of different personality traits are also aligned with the findings in Zhang et al. (2020). For example, most of the facets of N1-N6 negatively correlate with those of E1-E6 and C1-C6.

We have also found the factor loadings related to the sixth and seventh items (“Think highly of myself” and “Have a high opinion of myself”) which measure “A5 (modesty)” to be very large (6.48 and 7.38). Similarly, the factor loadings in the study by Zhang et al. (2020) are also large (4.19 and 4.41). When computing the polychoric correlation between the sixth and seventh items, we found an extremely large correlation coefficient (0.947), indicating local dependence between these two items.

The D-SOUL algorithm took 10 minutes and 47 seconds to estimate the model parameters. This included the time for both initialisation and subsequent stages. Despite the large sample size, number of items and latent dimensions, the algorithm showed high scalability. Additionally, two irregular aspects of the dataset contribute to slower parameter estimation. Firstly, there are two unusually large factor loadings. Secondly, the correlation matrix contains large values. These

features usually lead to slow parameter learning, requiring many iterations for convergence of the algorithm. Therefore, the short processing time under such a large-scale, and complex setting shows the high scalability of the D-SOUL algorithm.

6 Discussions

The paper proposes a new stochastic optimisation algorithm for marginal maximum likelihood estimation. Both simulation studies and a real data example demonstrated that the proposed algorithm is highly effective for estimating high-dimensional latent variable models. Specifically, in a real data example with 30,000 observation units, 300 items, and 30 latent variables, the proposed algorithm successfully converged to a sensible solution within 11 minutes. The success of the proposed algorithm is due to the use of two techniques – the unadjusted Langevin sampler and the minibatch stochastic gradient. Both techniques are relatively easy to implement.

The unadjusted Langevin sampler makes use of the geometric information of the target distribution, making it scalable with the dimension of the latent space. On the other hand, the minibatch stochastic gradient reduces the computational complexity of calculating the stochastic gradient, leading to faster convergence. In particular, the minibatch size of $n = 50, 100$ consistently performed well under all simulation conditions. However, a minibatch size of $n = 10$ resulted in slower convergence compared to $n = 50, 100$ in the confirmatory M2PL model, yet still showed faster convergence compared to other algorithms relying on a standard SG.

Based on the results from simulation and empirical studies, it is recommended to use $n = 50$ or 100 , as they provide the best statistical and computational efficiency. Furthermore, regarding the sensitivity of different tuning parameters, it was observed that the performance of the D-SOUL algorithm varied significantly among different tuning parameters. The theoretically driven step size of γ_t (e.g., $\gamma_t = \mu_1 t^{-0.84}$) decays quickly, making the convergence speed sensitive to the constant factor μ_1 , which rescales the magnitude of a decreasing sequence of γ_t . Hence, conducting an initialisation stage to obtain a good starting point using a fixed step size less sensitive to the choice of its constant factor is desirable, as the magnitude of the step size remains the same during the iterations.

While the proposed algorithm is promising for addressing the estimation problem in high-dimensional latent variable models, there is still room for improvement and exploration in several directions. One limitation is that the current algorithm cannot be directly applied to models with discrete latent variables due to the nature of the unadjusted Langevin sampler. This is important because many psychometric models involve discrete latent variables (e.g., [Henson et al., 2009](#); [Von Davier & Yamamoto, 2004](#)). Therefore, it would be valuable to extend the current algorithms to a more general setting that allows for both continuous and discrete latent variables. There has been recent developments in Langevin-like methods for MCMC analysis of models involving discrete

Table 1: Estimated factor loading parameters of the confirmatory M2PL model, IPIP-NEO dataset

Latent Traits	Factor Loading Parameters										
O1	1.67	1.75	2.79	2.30	1.38	1.02	2.35	1.56	1.53	1.61	
O2	2.85	0.79	1.51	0.96	1.30	3.27	1.59	2.25	0.55	0.96	
O3	2.10	1.14	0.58	0.35	0.52	2.15	2.42	1.21	1.61	1.50	
O4	1.19	0.97	0.86	1.39	1.39	2.46	2.47	1.07	0.68	1.13	
O5	1.13	1.78	1.49	1.18	1.13	1.61	1.96	2.06	2.28	1.84	
O6	1.57	0.77	1.37	0.77	2.00	0.62	1.23	1.42	1.67	0.97	
C1	1.68	1.87	1.96	1.46	1.82	2.17	1.34	1.39	1.64	1.02	
C2	1.91	1.85	0.85	1.66	1.42	1.52	1.75	1.56	1.15	1.47	
C3	1.56	1.49	1.02	1.70	1.26	1.83	1.61	1.42	1.52	1.28	
C4	1.33	2.35	1.57	1.40	1.81	1.28	0.86	1.43	2.02	2.04	
C5	1.65	1.48	2.21	2.01	1.48	2.62	2.19	2.25	2.89	1.44	
C6	0.78	0.93	0.72	2.83	2.00	1.30	2.38	1.46	2.92	1.16	
E1	2.19	1.69	3.15	2.64	1.61	1.43	1.98	2.26	1.12	1.64	
E2	2.34	2.05	1.60	1.40	1.21	2.03	1.98	2.52	2.86	1.69	
E3	2.57	2.17	1.19	1.05	2.26	2.04	1.64	1.47	1.13	1.25	
E4	1.87	2.00	1.62	1.10	0.59	0.87	0.72	0.70	0.64	0.72	
E5	2.27	2.11	1.95	1.50	1.59	1.88	1.14	1.54	1.09	0.96	
E6	1.88	2.58	1.00	1.29	2.26	2.16	1.40	1.24	1.13	0.98	
A1	2.26	2.22	2.60	1.72	1.90	1.05	3.20	1.58	1.16	1.68	
A2	0.93	1.07	0.80	1.59	0.97	1.66	1.10	1.14	2.55	1.45	
A3	1.69	1.24	1.83	1.99	1.12	1.31	1.47	1.29	1.52	1.73	
A4	0.63	0.62	0.77	1.18	1.10	1.06	1.78	2.13	1.56	1.09	
A5	0.66	0.80	0.90	0.58	1.45	6.48	7.38	0.82	0.66	0.81	
A6	1.46	1.78	0.86	1.11	1.50	1.38	0.72	1.11	0.93	0.89	
N1	1.71	1.51	1.65	2.55	1.61	1.59	1.49	1.23	1.32	1.19	
N2	2.74	2.30	2.45	1.62	2.35	2.82	2.33	2.27	1.52	1.20	
N3	2.32	2.81	2.83	2.72	1.61	1.91	1.37	1.77	2.03	2.02	
N4	1.49	1.14	1.99	1.62	1.43	0.98	1.37	1.16	1.54	1.37	
N5	0.98	1.09	1.22	1.26	0.58	1.43	1.47	1.54	0.78	0.61	
N6	2.28	1.62	2.04	1.15	1.69	2.12	1.30	1.64	1.67	2.15	

Note. The indicator matrix of the IPIP-NEO dataset has a simple structure. Accordingly, the values of each row represent the estimated factor loading parameters of ten items that load on the latent trait in that row.

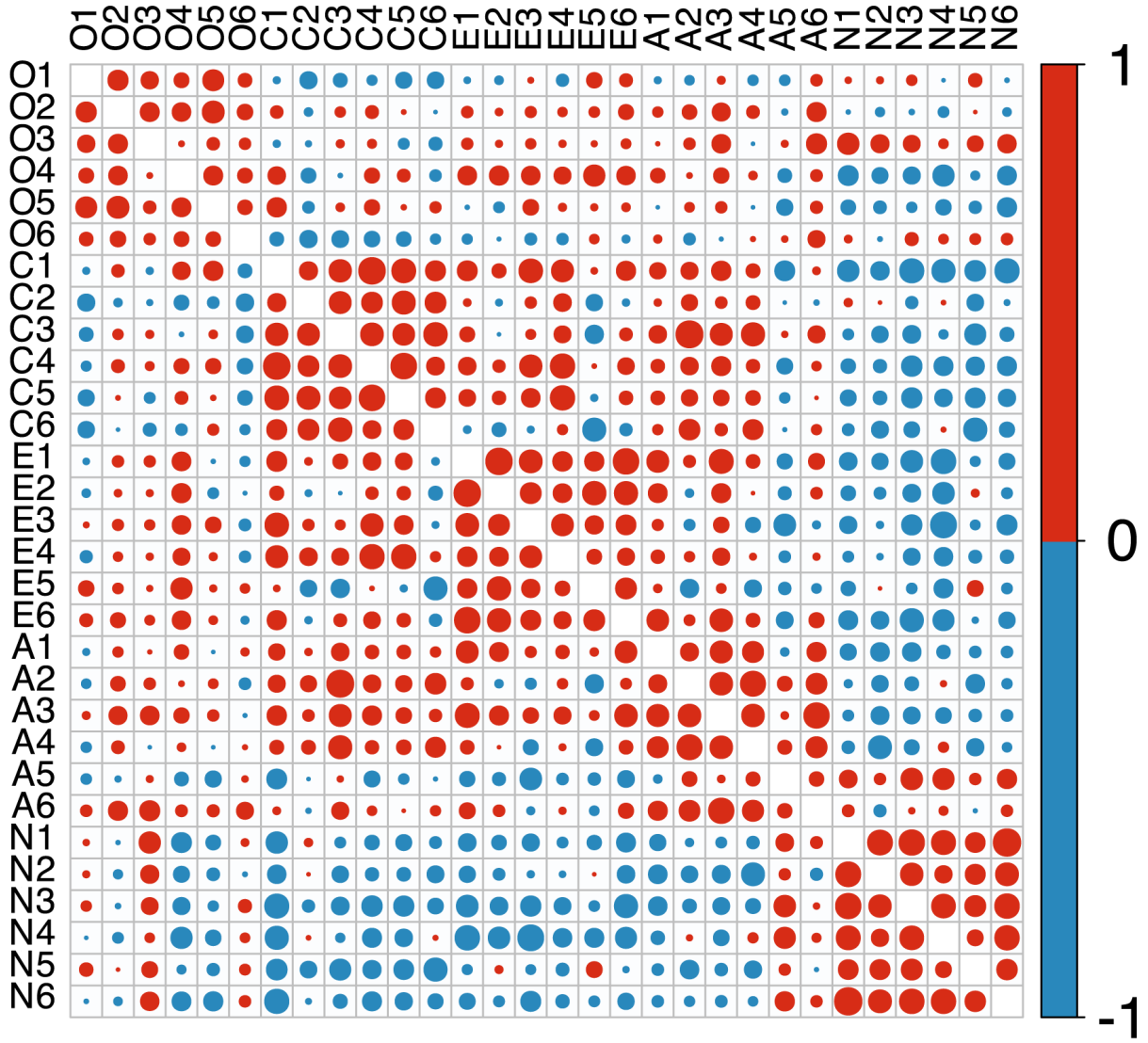


Figure 5: Estimated latent factor correlation matrix, IPIP-NEO dataset. Red and blue circles indicate positive and negative correlation coefficients, respectively, with the size of each circle corresponding to the magnitude of the coefficient.

variables (Zanella, 2020; Zhang et al., 2022) that use the geometric information of the target distribution to propose MCMC updates. These methods may be incorporated into the current framework to accommodate both continuous and discrete latent variables.

It is also important to consider extending the proposed algorithm to settings where the continuous latent variables are subject to specific equality and inequality constraints, which are commonly found in psychometric models. One example is the mixed membership model (Airoldi et al., 2015; Erosheva et al., 2004), where latent variables lie on a probability simplex. The unadjusted Langevin sampler does not handle sampling in constrained spaces. However, recent advancements in MCMC sampling have led to the development of mirror-Langevin methods (Hsieh et al., 2018) that enable efficient sampling from constrained spaces, including the probability simplex. These methods combine the unadjusted Langevin sampler with mirror descent methods for constrained optimization (Nemirovskij & Yudin, 1983) to achieve sampling in constrained spaces. It is possible to integrate mirror-Langevin methods into the current algorithm and develop the theoretical guarantee for the stochastic optimisation algorithm accordingly.

Finally, we note that several computational tricks proposed in Zhang and Chen (2022) can be incorporated into the current algorithm without difficulty, even though the current research did not explore these directions. Specifically, Zhang and Chen (2022) propose an adaptive method to construct $\mathbf{D}^{(t)}$, which, based on their simulation studies, leads to faster convergence. Additionally, they incorporate a stochastic proximal gradient update step for regularised marginal maximum likelihood estimation, where the objective function involves a LASSO-type non-smooth penalty term. We plan to include these techniques into the D-SOUL algorithm in our future work.

In summary, the proposed D-SOUL algorithm is easy to implement, theoretically sound, potentially applicable to a wide range of latent variable models, and scales effectively as the dimension of the latent space increases. It paves the way for estimating high-dimensional latent variable models, which are becoming more prevalent in social and behavioural research.

Supplementary Materials

A.1 Proof of Theorem 1

First, we introduce the notations based on [De Bortoli et al. \(2021\)](#). Denote by $\mathcal{B}(\mathbb{R}^K)$ the Borel σ -field of \mathbb{R}^K . For a probability measure μ on $(\mathbb{R}^K, \mathcal{B}(\mathbb{R}^K))$ and a μ -integrable function f , denote by $\mathbb{E}_\mu[f]$ the integral of f with respect to μ . For $f : \mathbb{R}^K \rightarrow \mathbb{R}$ measurable, the V -norm of f is given by $\|f\|_V = \sup_{\xi_i \in \mathbb{R}^K} |f(\xi_i)|/V(\xi_i)$. Let μ' be a finite signed measure on $(\mathbb{R}^K, \mathcal{B}(\mathbb{R}^K))$. The V -total variation distance of μ' is defined as

$$\|\mu'\|_V = \sup_{\|f\|_V \leq 1} \left| \int_{\mathbb{R}^K} f(\xi_i) d\mu'(\xi_i) \right|.$$

We also define the total variation distance of finite signed measure μ' by $\|\mu'\|_{TV}$, by which we have $\|\mu'\|_V = \|V \cdot \mu'\|_{TV}$. For any $a \in \mathbb{R}^K$ and $R > 0$, denote by $B(a, R)$ the open ball centered at a with radius R . Let (X, \mathcal{X}) and (Y, \mathcal{Y}) be two measurable spaces. A Markov kernel K is a mapping $K : X \times \mathcal{Y} \rightarrow [0, 1]$ such that for any $x \in X$, $K(x, \cdot)$ is a probability measure and for any $A \in \mathcal{Y}$, $K(\cdot, A)$ is measurable. We also denote by δ_{ξ_i} the Dirac mass at $\xi_i \in \mathbb{R}^K$. The complement of a set $A \subset \mathbb{R}^K$ is denoted by A^c . All densities are w.r.t. the Lebesgue measure unless stated otherwise.

Additionally, we define notation for the posterior distribution of the latent variables, the gradient of an objective function, and standard/minibatch stochastic gradients (SGs). First, the posterior distribution for the i -th observation is a function of model parameters given the observed data defined as

$$p_{\beta,i}(\xi_i) = \frac{f_i(\mathbf{Y}_i, \xi_i | \beta)}{\int f_i(\mathbf{Y}_i, \tilde{\xi}_i | \beta) d\tilde{\xi}_i},$$

where the joint posterior distribution of the latent variables for all N observations is denoted by $\pi_\beta(\boldsymbol{\xi}) = \prod_{i=1}^N p_{\beta,i}(\xi_i)$ and the posterior distribution at the t -th iteration is written as $p_{\beta^{(t-1)},i}(\xi_i^{(t)})$. a function proportional to $p_{\beta,i}(\xi_i)$ (potential function) is defined as

$$U_{\beta,i}(\xi_i) = -\log\{f_i(\mathbf{Y}_i, \xi_i | \beta)\},$$

where $p_{\beta,i}(\xi_i) \propto e^{-U_{\beta,i}(\xi_i)}$.

Second, denote the i -th contribution of the gradient of an objective function, $\nabla_\beta l(\beta)$, by

$$\nabla_{\beta,i} l(\beta) = \nabla_\beta \log \left(\int f_i(\mathbf{Y}_i, \xi_i | \beta) d\xi_i \right),$$

and $\nabla_\beta l(\beta) = \sum_{i=1}^N \nabla_{\beta,i} l(\beta)$. Similarly, the standard SG is the sum of N gradients, each of which

is a function of the sampled latent variables for observation i and model parameters defined by

$$\mathbf{G}_{\beta,i}(\boldsymbol{\xi}_i) = \left(\frac{\partial \log \{f_i(\mathbf{Y}_i, \boldsymbol{\xi}_i | \boldsymbol{\beta})\}}{\partial \boldsymbol{\beta}} \right) \Big|_{\boldsymbol{\beta}=\boldsymbol{\beta}}.$$

Then, the standard SG is defined as

$$\mathbf{G}_{\beta}(\boldsymbol{\xi}) = \sum_{i=1}^N \mathbf{G}_{\beta,i}(\boldsymbol{\xi}_i).$$

A function of the minibatch SG is also defined similarly by

$$\mathbf{G}_{\beta}^{\text{mini}}(\boldsymbol{\xi}, S) = \frac{N}{n} \sum_{i=1}^N \mathbb{1}_{\{i \in S\}} \mathbf{G}_{\beta,i}(\boldsymbol{\xi}_i).$$

Furthermore, the expectations using $\pi_{\beta}(\boldsymbol{\xi})$, $p_{\beta,h,i}(\boldsymbol{\xi}_i)$, and $p_{\beta,i}(\boldsymbol{\xi}_i)$ are denoted as $\mathbb{E}_{\pi_{\beta}}[\cdot]$, $\mathbb{E}_{p_{\beta,h,i}}[\cdot]$, and $\mathbb{E}_{p_{\beta,i}}[\cdot]$, respectively. A Markov kernel for $p_{\beta,h,i}(\boldsymbol{\xi}_i)$ that is associated with step size h and model parameter $\boldsymbol{\beta}$ and obtained after n MCMC iterations is also denoted by $K_{\beta,h,i}^n$. For example, the Markov kernel after one MCMC iteration, which corresponds to our setting, is written as $K_{\beta,h,i}^1$. Moreover, the expectation using Markov kernel $K_{\beta,h,i}^n$ on $\mathbf{G}_{\beta,i}(\boldsymbol{\xi}_i)$ is denoted $K_{\beta,h,i}^n \mathbf{G}_{\beta,i}(\boldsymbol{\xi}_i)$, and we write $K_{\beta,h}^n \mathbf{G}_{\beta}(\boldsymbol{\xi}) = \sum_{i=1}^N K_{\beta,h,i}^n \mathbf{G}_{\beta,i}(\boldsymbol{\xi}_i)$. Additionally, $\mathcal{F}_t = \sigma(\boldsymbol{\beta}^{(0)}, \{\boldsymbol{\xi}^{(\ell)}, S^{(\ell)}, \ell \in \{1, \dots, t\}\})$ is a filtration of σ -algebra.

Next, we provide the assumptions for the convergence of the sequence $\boldsymbol{\beta}^{(t)}$ to the MMLE $\hat{\boldsymbol{\beta}}$. Our theoretical results are primarily based on the assumptions introduced in [De Bortoli et al. \(2021\)](#), and some assumptions are adapted from their study. Our theoretical convergence study considers the case where the objective function $-l(\boldsymbol{\beta})$ is convex. However, we can easily extend the theoretical convergence result to a non-convex case by capitalizing Theorem S19 in the Supplementary Materials of [De Bortoli et al. \(2021\)](#), which addresses convergence under a non-convex objective function.

Assumption 1 *Elements of a minibatch $S^{(t)}$, which is a subset of $\{1, \dots, N\}$ of size n , are randomly sampled from discrete uniform distribution $\text{DiscreteUniform}(1, N)$. In addition, $(S^{(t)})_{t \in \mathbb{N}}$ are independent.*

Assumption 2 (1) *The parameter space \mathcal{B} is compact and convex.*

(2) *For any $\boldsymbol{\beta}_1, \boldsymbol{\beta}_2 \in \mathcal{B}$, there exists $L_1 \geq 0$ such that*

$$\|\nabla_{\boldsymbol{\beta}_1} l(\boldsymbol{\beta}_1) - \nabla_{\boldsymbol{\beta}_2} l(\boldsymbol{\beta}_2)\| \leq L_1 \|\boldsymbol{\beta}_1 - \boldsymbol{\beta}_2\|.$$

(3) *For any $\boldsymbol{\beta} \in \mathcal{B}$ and $\boldsymbol{\xi}_i \in \mathbb{R}^K$, $\mathbf{G}_{\beta,i}(\boldsymbol{\xi}_i)$ is well defined. In addition, a probability distribution*

$p_{\beta,i}$ satisfies that $\mathbb{E}_{p_{\beta,i}}[\|\mathbf{G}_{\beta,i}(\boldsymbol{\xi}_i)\|] < +\infty$,

$$\nabla_{\beta,i}l(\boldsymbol{\beta}) = \mathbb{E}_{p_{\beta,i}}[\mathbf{G}_{\beta,i}(\boldsymbol{\xi}_i)],$$

and

$$\begin{aligned}\nabla_{\boldsymbol{\beta}}l(\boldsymbol{\beta}) &= \mathbb{E}_{\pi_{\boldsymbol{\beta}}}[\mathbf{G}_{\boldsymbol{\beta}}(\boldsymbol{\xi})] \\ &= \sum_{i=1}^N \mathbb{E}_{p_{\beta,i}}[\mathbf{G}_{\beta,i}(\boldsymbol{\xi}_i)].\end{aligned}$$

Assumption 3 There exists $L_2 \geq 0$ such that for $\boldsymbol{\beta}_1, \boldsymbol{\beta}_2 \in \mathcal{B}$ and $\boldsymbol{\xi}_i \in \mathbb{R}^K$, $\|\mathbf{G}_{\boldsymbol{\beta}_1,i}(\boldsymbol{\xi}_i) - \mathbf{G}_{\boldsymbol{\beta}_2,i}(\boldsymbol{\xi}_i)\| \leq L_2\|\boldsymbol{\beta}_1 - \boldsymbol{\beta}_2\|V^{1/2}(\boldsymbol{\xi}_i)$, where V is a measurable bounded function of $\boldsymbol{\xi}_i \mapsto [1, +\infty)$ satisfying the conditions in Proposition 1 introduced later.

We further provide the assumptions on the family of probability distributions $(p_{\beta,i})_{\beta \in \mathcal{B}}$ for a Markov process in an unadjusted Langevin sampling (ULS) step.

Assumption 4 For any $\boldsymbol{\beta} \in \mathcal{B}$, there exists $U_{\beta,i} : \mathbb{R}^K \rightarrow \mathbb{R}$ such that $p_{\beta,i}$ admits a probability density function proportional to $\boldsymbol{\xi}_i \mapsto \exp[-U_{\beta,i}(\boldsymbol{\xi}_i)]$. In addition, $(\boldsymbol{\beta}, \boldsymbol{\xi}_i) \mapsto U_{\beta,i}(\boldsymbol{\xi}_i)$ is continuous, $\boldsymbol{\xi}_i \mapsto U_{\beta,i}(\boldsymbol{\xi}_i)$ is differentiable for all $\boldsymbol{\beta} \in \mathcal{B}$, and there exists $L_3 \geq 0$ such that for any $\boldsymbol{\xi}_i, \boldsymbol{\xi}'_i \in \mathbb{R}^K$,

$$\sup_{\boldsymbol{\beta} \in \mathcal{B}} \|\nabla_{\boldsymbol{\xi}_i} U_{\beta,i}(\boldsymbol{\xi}_i) - \nabla_{\boldsymbol{\xi}_i} U_{\beta,i}(\boldsymbol{\xi}'_i)\| \leq L_3 \|\boldsymbol{\xi}_i - \boldsymbol{\xi}'_i\|$$

and $\{\|\nabla_{\boldsymbol{\xi}_i} U_{\beta,i}(\mathbf{0}) : \boldsymbol{\beta} \in \mathcal{B}\|\}$ is bounded.

Assumption 5 There exist $m_1, m_2 > 0$ and $c, R_1 \geq 0$ such that for any $\boldsymbol{\beta} \in \mathcal{B}$ and $\boldsymbol{\xi}_i \in \mathbb{R}^K$,

$$\langle \nabla_{\boldsymbol{\xi}_i} U_{\beta,i}(\boldsymbol{\xi}_i), \boldsymbol{\xi}_i \rangle \geq m_1 \|\boldsymbol{\xi}_i\| \mathbb{1}_{B(0, R_1)^c}(\boldsymbol{\xi}_i) + m_2 \|\nabla_{\boldsymbol{\xi}_i} U_{\beta,i}(\boldsymbol{\xi}_i)\|^2 - c.$$

Assumption 6 There exists $L_4 \geq 0$ such that for any $\boldsymbol{\xi}_i \in \mathbb{R}^K$, $\boldsymbol{\beta}_1, \boldsymbol{\beta}_2 \in \mathcal{B}$,

$$\|\nabla_{\boldsymbol{\xi}_i} U_{\boldsymbol{\beta}_1}(\boldsymbol{\xi}_i) - \nabla_{\boldsymbol{\xi}_i} U_{\boldsymbol{\beta}_2}(\boldsymbol{\xi}_i)\| \leq L_4 \|\boldsymbol{\beta}_1 - \boldsymbol{\beta}_2\| V^{1/2}(\boldsymbol{\xi}_i).$$

Next, we provide Propositions based on De Bortoli et al. (2021), which are required for the stability of a Markov process in an ULS step.

Proposition 1 Assume Assumptions 4-5. Then, there exists a measurable function $V : \mathbb{R}^K \rightarrow [1, +\infty)$ satisfying the following conditions.

(1) There exists $A_1 \geq 1$ such that for any $t, n \in \mathbb{N}$,

$$\mathbb{E}\left[K_{\boldsymbol{\beta}^{(t)}, h_t, i}^n V(\boldsymbol{\xi}_i^{(t)}) | \boldsymbol{\xi}_i^{(0)}\right] \leq A_1 V(\boldsymbol{\xi}_i^{(0)})$$

$$\mathbb{E}\left[V\left(\boldsymbol{\xi}_i^{(0)}\right)\right] < +\infty.$$

(2) For any $h \in (0, \bar{h}]$, $\boldsymbol{\beta} \in \mathcal{B}$, $K_{\boldsymbol{\beta}, h, i}$ admits a stationary distribution $p_{\boldsymbol{\beta}, h, i}$, and there exist $A_2, A_3 \geq 1, \rho \in [0, 1)$ such that for any $h \in (0, \bar{h}]$, $\boldsymbol{\beta} \in \mathcal{B}$, $\boldsymbol{\xi}_i \in \mathbb{R}^K$ and $n \in \mathbb{N}$

$$\begin{aligned} \left\| \delta_{\boldsymbol{\xi}_i} K_{\boldsymbol{\beta}, h, i}^n - p_{\boldsymbol{\beta}, h, i} \right\|_V &\leq A_2 \rho^{nh} V(\boldsymbol{\xi}_i) \\ p_{\boldsymbol{\beta}, h, i}(V) &\leq A_3 \end{aligned}$$

(3) There exists $\Psi : \mathbb{R}_+^* \rightarrow \mathbb{R}_+$ such that for any $h \in (0, \bar{h}]$ and $\boldsymbol{\beta} \in \mathcal{B}$

$$\|p_{\boldsymbol{\beta}, h, i} - p_{\boldsymbol{\beta}, i}\|_{V^{1/2}} \leq \Psi(h).$$

Proof. Under Assumptions 4 and 5, Theorem 7 in De Bortoli et al. (2021) shows that the conditions (1)-(3) in Proposition 1 hold by letting $V = \exp\left[m_1 \sqrt{1 + \|\boldsymbol{\xi}_i\|^2}/4\right]$, $\bar{h} = \min(1, 2m_2)$, and $\Psi(\gamma) = D_4 \sqrt{\bar{h}}$, where D_4 is provided in Proposition S15 in Supplementary Materials of De Bortoli et al. (2021).

Proposition 2 Assume Assumptions 4-6 and $\|\mathbf{G}_{\boldsymbol{\beta}, i}(\boldsymbol{\xi}_i)\| \leq V^{1/4}(\boldsymbol{\xi}_i)$ for any $\boldsymbol{\beta} \in \mathcal{B}$ and any $\boldsymbol{\xi}_i \in \mathbb{R}^K$. Then, there exists $\boldsymbol{\Lambda}_1 : (\mathbb{R}_+^*)^2 \rightarrow \mathbb{R}_+$ and $\boldsymbol{\Lambda}_2 : (\mathbb{R}_+^*)^2 \rightarrow \mathbb{R}_+$ such that for any $h_1, h_2 \in (0, \bar{h}]$ with $h_2 < h_1$, $\boldsymbol{\beta}_1, \boldsymbol{\beta}_2 \in \mathcal{B}$, $\boldsymbol{\xi}_i \in \mathbb{R}^K$ and $a \in [1/4, 1/2]$,

$$\|\delta_{\boldsymbol{\xi}_i} K_{\boldsymbol{\beta}_1, h_1, i} - \delta_{\boldsymbol{\xi}_i} K_{\boldsymbol{\beta}_2, h_2, i}\|_{V^a} \leq [\boldsymbol{\Lambda}_1(h_1, h_2) + \boldsymbol{\Lambda}_2(h_1, h_2) \|\boldsymbol{\beta}_1 - \boldsymbol{\beta}_2\|] V^{2a}(\boldsymbol{\xi}_i).$$

Proof. Under Assumptions 4-6 and with $V = \exp\left[m_1 \sqrt{1 + \|\boldsymbol{\xi}_i\|^2}/4\right]$, $\|\mathbf{G}_{\boldsymbol{\beta}, i}(\boldsymbol{\xi}_i)\| \leq V^{1/4}(\boldsymbol{\xi}_i)$ for any $\boldsymbol{\beta} \in \mathcal{B}$ and $\boldsymbol{\xi}_i \in \mathbb{R}^K$, Theorem 8 in De Bortoli et al. (2021) shows that Proposition 2 holds by letting $\bar{h} = \min(1, 2m_2)$ and for any $h_1, h_2 \in (0, \bar{h}]$, $h_2 < h_1$, $\boldsymbol{\Lambda}_1(h_1, h_2) = D_5(h_1/h_2 - 1)$ and $\boldsymbol{\Lambda}_2(h_1, h_2) = D_5 h_2^{1/2}$, where D_5 is given in Proposition S16 in De Bortoli et al. (2021).

These Propositions are required to ensure the stability of a Markov process driven by the unadjusted Langevin sampler. In particular, Proposition 1-(2) means that the Markov kernel $K_{\boldsymbol{\beta}, h, i}$ satisfies an ergodicity condition in V -norm uniformly in model parameter $\boldsymbol{\beta}$ (De Bortoli et al., 2021). The ergodicity condition is usually required to obtain the desired properties of an MCMC method, such as the central limit theorem for a Markov chain (Jarner & Hansen, 2000). In our case, this condition is necessary to control the bias of an SG induced by approximate posterior sampling, which is required to guarantee the convergence of model parameter $\boldsymbol{\beta}$. Proposition 1-(3) is introduced to control the distance between the invariant distribution of the Markov kernel $K_{\boldsymbol{\beta}, h, i}$ and the target distribution $p_{\boldsymbol{\beta}, i}$ uniformly in the model parameter $\boldsymbol{\beta}$ (De Bortoli et al., 2021).

Next, define for any $t \in \mathbb{N}$,

$$\eta_t = \mathbf{G}_{\beta^{(t-1)}}^{\text{mini}}(\boldsymbol{\xi}^{(t)}, S^{(t)}) - \mathbf{G}_{\beta^{(t-1)}}(\boldsymbol{\xi}^{(t)}) + \left(\mathbf{G}_{\beta^{(t-1)}}(\boldsymbol{\xi}^{(t)}) - \mathbb{E}_{\pi_{\beta^{(t-1)}}} \left[\mathbf{G}_{\beta^{(t-1)}}(\boldsymbol{\xi}^{(t)}) \right] \right). \quad (9)$$

We denote the first two terms on the right-hand side of (9) by $\eta_t^{(1)} = \mathbf{G}_{\beta^{(t-1)}}^{\text{mini}}(\boldsymbol{\xi}^{(t)}, S^{(t)}) - \mathbf{G}_{\beta^{(t-1)}}(\boldsymbol{\xi}^{(t)})$ and the term in the parenthesis by $\eta_t^{(2)} = \mathbf{G}_{\beta^{(t-1)}}(\boldsymbol{\xi}^{(t)}) - \mathbb{E}_{\pi_{\beta^{(t-1)}}} \left[\mathbf{G}_{\beta^{(t-1)}}(\boldsymbol{\xi}^{(t)}) \right]$. Then, we write $\eta_t = \eta_t^{(1)} + \eta_t^{(2)}$.

Subsequently, we first focus on $\eta_t^{(2)}$, which can be rewritten as

$$\begin{aligned} \eta_t^{(2)} &= \mathbf{G}_{\beta^{(t-1)}}(\boldsymbol{\xi}^{(t)}) - \mathbb{E}_{\pi_{\beta^{(t-1)}}} \left[\mathbf{G}_{\beta^{(t-1)}}(\boldsymbol{\xi}^{(t)}) \right] \\ &= \sum_{i=1}^N \left\{ \mathbf{G}_{\beta^{(t-1)},i}(\boldsymbol{\xi}_i^{(t)}) - \mathbb{E}_{p_{\beta^{(t-1)},i}} \left[\mathbf{G}_{\beta^{(t-1)},i}(\boldsymbol{\xi}_i^{(t)}) \right] \right\} \\ &= \sum_{i=1}^N \eta_t^{(2),i}, \end{aligned}$$

where we define $\eta_t^{(2),i} = \mathbf{G}_{\beta^{(t-1)},i}(\boldsymbol{\xi}_i^{(t)}) - \mathbb{E}_{p_{\beta^{(t-1)},i}} \left[\mathbf{G}_{\beta^{(t-1)},i}(\boldsymbol{\xi}_i^{(t)}) \right]$. Note that $\eta_t^{(2),i}$ is identical to Equation S20 in Supplementary Materials of [De Bortoli et al. \(2021\)](#) by letting $H_{\tilde{\theta}_n}(\tilde{X}_{n+1}) = \mathbf{G}_{\beta^{(t-1)},i}(\boldsymbol{\xi}_i^{(t)})$ and $\pi_{\tilde{\theta}_n}(H_{\tilde{\theta}_n}) = \mathbb{E}_{p_{\beta^{(t-1)},i}} \left[\mathbf{G}_{\beta^{(t-1)},i}(\boldsymbol{\xi}_i^{(t)}) \right]$ in Equation S20. Then, by Assumption 3 and Proposition 1-(1)-(2), for any $\beta \in \mathcal{B}$ and $h \in (0, \bar{h}]$, there exists a function $\mathbf{G}_{\beta,h,i}^* : \mathbb{R}^K \rightarrow \mathbb{R}^p$ solution of the Poisson equation,

$$(\mathbf{I}_p - K_{\beta,h,i}) \mathbf{G}_{\beta,h,i}^* = \mathbf{G}_{\beta,i}(\boldsymbol{\xi}_i) - \mathbb{E}_{p_{\beta,h,i}} \left[\mathbf{G}_{\beta,i}(\boldsymbol{\xi}_i) \right], \quad (10)$$

defined for any $\boldsymbol{\xi}_i \in \mathbb{R}^K$ by

$$\mathbf{G}_{\beta,h,i}^*(\boldsymbol{\xi}_i) = \sum_{j \in \mathbb{N}} \left\{ K_{\beta,h,i}^j \mathbf{G}_{\beta,i}(\boldsymbol{\xi}_i) - \mathbb{E}_{p_{\beta,h,i}} \left[\mathbf{G}_{\beta,i}(\boldsymbol{\xi}_i) \right] \right\},$$

where \mathbf{I}_p is an identity matrix. Using (10), which corresponds to Equation S17 in Supplementary Materials of [De Bortoli et al. \(2021\)](#), $\eta_t^{(2),i}$ can be decomposed into four parts (Equation S21 in Supplementary Materials; [De Bortoli et al., 2021](#)):

$$\eta_t^{(2),i} = \eta_t^{(2),(a),i} + \eta_t^{(2),(b),i} + \eta_t^{(2),(c),i} + \eta_t^{(2),(d),i},$$

where

$$\begin{aligned} \eta_t^{(2),(a),i} &= \mathbf{G}_{\beta^{(t-1)},h_t,i}^*(\boldsymbol{\xi}_i^{(t)}) - K_{\beta^{(t-1)},h_t,i}^1 \mathbf{G}_{\beta^{(t-1)},h_t,i}^*(\boldsymbol{\xi}_i^{(t-1)}) \\ \eta_t^{(2),(b),i} &= K_{\beta^{(t-1)},h_t,i}^1 \mathbf{G}_{\beta^{(t-1)},h_t,i}^*(\boldsymbol{\xi}_i^{(t-1)}) - K_{\beta^{(t)},h_{t+1},i}^1 \mathbf{G}_{\beta^{(t)},h_{t+1},i}^*(\boldsymbol{\xi}_i^{(t)}) \end{aligned}$$

$$\begin{aligned}\eta_t^{(2),(c),i} &= K_{\beta^{(t)},h_{t+1},i}^{-1} \mathbf{G}_{\beta^{(t)},h_{t+1},i}^* (\boldsymbol{\xi}_i^{(t)}) - K_{\beta^{(t-1)},h_t,i}^{-1} \mathbf{G}_{\beta^{(t-1)},h_t,i}^* (\boldsymbol{\xi}_i^{(t)}) \\ \eta_t^{(2),(d),i} &= \mathbb{E}_{p_{\beta^{(t-1)},h_t,i}} [\mathbf{G}_{\beta^{(t-1)},i} (\boldsymbol{\xi}_i^{(t)})] - \mathbb{E}_{p_{\beta^{(t-1)},i}} [\mathbf{G}_{\beta^{(t-1)},i} (\boldsymbol{\xi}_i^{(t)})]\end{aligned}$$

To establish Theorem 1, we need to verify that Theorem 2 in [Atchade et al. \(2017\)](#) holds in our setting. In the same manner as Proof (a) for Theorem 5 of [De Bortoli et al. \(2021\)](#), we can verify this by checking if the following series converge almost surely (a.s)

$$\sum_{t=1}^{+\infty} \gamma_t \langle \Pi_{\mathcal{B}} [\boldsymbol{\beta}^{(t-1)} + \gamma_t \nabla_{\boldsymbol{\beta}} l(\boldsymbol{\beta}^{(t-1)})] - \hat{\boldsymbol{\beta}}, \eta_t^{(1)} \rangle, \quad (11)$$

$$\sum_{t=1}^{+\infty} \gamma_t \langle \Pi_{\mathcal{B}} [\boldsymbol{\beta}^{(t-1)} + \gamma_t \nabla_{\boldsymbol{\beta}} l(\boldsymbol{\beta}^{(t-1)})] - \hat{\boldsymbol{\beta}}, \eta_t^{(2),(q),i} \rangle \text{ for } q \in \{1, 2, 3, 4\} \text{ and } i \in \{1, \dots, N\}, \quad (12)$$

$$\sum_{t=1}^{+\infty} \gamma_t^2 \|\eta_t\|^2, \quad (13)$$

with $\hat{\boldsymbol{\beta}} \in \operatorname{argmax}_{\boldsymbol{\beta} \in \mathcal{B}} l(\boldsymbol{\beta})$. Here, $\Pi_{\mathcal{B}}$ is the projection onto \mathcal{B} , which is required to ensure $\boldsymbol{\beta} \in \mathcal{B}$. Note that the implementation of the D-SOUL algorithm does not need the projection (that can be addressed by the quasi-Newton proximal update with $\mathbf{D}^{(t)}$ being the identity matrix) unless there is a specific parameter constraint, such as in the correlation matrix of the M2PL model. This is because a set of possible values for numerical computations is bounded and convex, except for the numerically unstable case of values taking on ∞ .

First, by Assumptions 2-6 and Propositions 1-2, $\|\mathbf{G}_{\beta,i}(\boldsymbol{\xi}_i)\| \leq V^{1/4}(\boldsymbol{\xi}_i)$ for any $\boldsymbol{\beta} \in \mathcal{B}$ and $\boldsymbol{\xi}_i \in \mathbb{R}^K$, using $\sum_{t \in \mathbb{N}} \gamma_t^2/h_t^2 < +\infty$ and Lemmas S6-S9 in Supplementary Materials of [De Bortoli et al. \(2021\)](#), Proof (a) for Theorem 5 of [De Bortoli et al. \(2021\)](#) guarantees that the series in (12) converges a.s for all q and i .

Second, using the Cauchy–Schwarz inequality, triangular inequalities, and $(a+b)^2 \leq 2(a^2+b^2)$ for $a, b \in \mathbb{R}$, the series in (13) can be rewritten as

$$\begin{aligned}\sum_{t=1}^{+\infty} \gamma_t^2 \|\eta_t\|^2 &\leq \sum_{t=1}^{+\infty} \gamma_t^2 \cdot \left\{ \|\eta_t^{(1)}\| + \|\eta_t^{(2)}\| \right\}^2 \\ &\leq \sum_{t=1}^{+\infty} \gamma_t^2 \cdot 2 \left\{ \|\eta_t^{(1)}\|^2 + \|\eta_t^{(2)}\|^2 \right\} \\ &\leq \sum_{t=1}^{+\infty} \gamma_t^2 \cdot 2 \left\{ \|\eta_t^{(1)}\|^2 + \left\{ \sum_{i=1}^N \|\eta_t^{(2),i}\| \right\}^2 \right\} \\ &\leq \sum_{t=1}^{+\infty} \gamma_t^2 \cdot 2 \left\{ \|\eta_t^{(1)}\|^2 + N \left(\sum_{i=1}^N \|\eta_t^{(2),i}\|^2 \right) \right\} \\ &= 2 \sum_{t=1}^{+\infty} \gamma_t^2 \|\eta_t^{(1)}\|^2 + 2N \sum_{t=1}^{+\infty} \sum_{i=1}^N \gamma_t^2 \|\eta_t^{(2),i}\|^2.\end{aligned} \quad (14)$$

Here, from Proof (a) for Theorem 5 of [De Bortoli et al. \(2021\)](#), which uses Lemma S5 in their Supplementary Materials, $\sum_{t=1}^{+\infty} \gamma_t^2 \left\| \eta_t^{(2),i} \right\|^2$ is convergent for all i . Thus,

$$\sum_{t=1}^{+\infty} \sum_{i=1}^N \gamma_t^2 \left\| \eta_t^{(2),i} \right\|^2 = \sum_{i=1}^N \sum_{t=1}^{+\infty} \gamma_t^2 \left\| \eta_t^{(2),i} \right\|^2,$$

which gives that $\sum_{t=1}^{+\infty} \gamma_t^2 \left\| \eta_t^{(2)} \right\|^2$ converges a.s.

Regarding the first term $\sum_{t=1}^{+\infty} \gamma_t^2 \left\| \eta_t^{(1)} \right\|^2$ in the right-hand side of the inequality (14), using $(a+b)^2 \leq 2(a^2 + b^2)$ for $a, b \in \mathbb{R}$ and triangular inequality, we have

$$\begin{aligned} \left\| \eta_t^{(1)} \right\|^2 &= \left\| \mathbf{G}_{\beta^{(t-1)}}^{\text{mini}}(\boldsymbol{\xi}^{(t)}, S^{(t)}) - \mathbf{G}_{\beta^{(t-1)}}(\boldsymbol{\xi}^{(t)}) \right\|^2 \\ &\leq 2 \left\{ \left\| \mathbf{G}_{\beta^{(t-1)}}^{\text{mini}}(\boldsymbol{\xi}^{(t)}, S^{(t)}) \right\|^2 + \left\| \mathbf{G}_{\beta^{(t-1)}}(\boldsymbol{\xi}^{(t)}) \right\|^2 \right\}. \end{aligned}$$

Here, by $\left\| \mathbf{G}_{\beta,i}(\boldsymbol{\xi}_i) \right\| \leq V^{1/4}(\boldsymbol{\xi}_i)$ for any $\beta \in \mathcal{B}$ and $\boldsymbol{\xi}_i \in \mathbb{R}^K$, the upper bound of $\left\| \mathbf{G}_{\beta^{(t-1)}}^{\text{mini}}(\boldsymbol{\xi}^{(t)}, S^{(t)}) \right\|^2$ is given as

$$\begin{aligned} \left\| \mathbf{G}_{\beta^{(t-1)}}^{\text{mini}}(\boldsymbol{\xi}^{(t)}, S^{(t)}) \right\|^2 &= \left\| \sum_{i \in S^{(t)}} \mathbf{G}_{\beta^{(t-1)},i}(\boldsymbol{\xi}_i) \right\|^2 \\ &\leq \left\{ \sum_{i \in S^{(t)}} \left\| \mathbf{G}_{\beta^{(t-1)},i}(\boldsymbol{\xi}_i^{(t)}) \right\| \right\}^2 \\ &\leq \left\{ \sum_{i \in S^{(t)}} V^{1/4}(\boldsymbol{\xi}_i^{(t)}) \right\}^2 \\ &\leq n^2 C_1 \end{aligned}$$

where C_1 is some positive constant. The above inequality is obtained because $V : \mathbb{R}^K \rightarrow [1, +\infty)$ is a bounded function. In addition, we also have

$$\begin{aligned} \left\| \mathbf{G}_{\beta^{(t-1)}}(\boldsymbol{\xi}^{(t)}) \right\|^2 &\leq \left\{ \sum_{i=1}^N V^{1/4}(\boldsymbol{\xi}_i^{(t)}) \right\}^2 \\ &\leq N^2 C_1. \end{aligned}$$

Thus, we have $\left\| \eta_t^{(1)} \right\|^2 \leq 2C_1(n + N)$. Accordingly, since $\sum_{t=1}^{\infty} \gamma_t^2 < +\infty$ by definition, the series $\sum_{t=1}^{+\infty} \gamma_t^2 \left\| \eta_t^{(1)} \right\|^2$ converges absolutely. Hence, the series in (13) converges a.s.

Lastly, regarding the series in (11), by Assumption 1, $\eta_t^{(1)}$ is unbiased in the sense that $\mathbb{E}[\eta_t^{(1)} | \mathcal{F}_t] = 0$. Thus, we can apply the Proposition 18 of [Atchade et al. \(2017\)](#) to these unbi-

ased terms. In particular, we need to show that

$$\sum_{t=1}^{+\infty} \gamma_t \langle \Pi_{\mathcal{B}} [\boldsymbol{\beta}^{(t-1)} + \gamma_t \nabla_{\boldsymbol{\beta}} l(\boldsymbol{\beta}^{(t-1)})] - \hat{\boldsymbol{\beta}}, \eta_t^{(1)} \rangle \quad (15)$$

converge a.s. Here, define

$$M_n^{(1)} = \sum_{t=1}^n \gamma_t \langle \Pi_{\mathcal{B}} [\boldsymbol{\beta}^{(t-1)} + \gamma_t \nabla_{\boldsymbol{\beta}} l(\boldsymbol{\beta}^{(t-1)})] - \hat{\boldsymbol{\beta}}, \eta_t^{(1)} \rangle.$$

Since $\mathbb{E}[\eta_t^{(1)} | \mathcal{F}_t] = 0$, $\{M_n^{(1)}\}_{n \in \mathbb{N}}$ is a martingale. This martingale converge a.s if

$$S^{(1)} = \sum_{t=1}^{+\infty} \gamma_t^2 \left\| \Pi_{\mathcal{B}} [\boldsymbol{\beta}^{(t-1)} + \gamma_t \nabla_{\boldsymbol{\beta}} l(\boldsymbol{\beta}^{(t-1)})] - \hat{\boldsymbol{\beta}} \right\|^2 \|\eta_t^{(1)}\|^2 < +\infty \quad \mathbb{P}\text{-a.s.}$$

First, for any $t \in \mathbb{N}$, $\left\| \Pi_{\mathcal{B}} [\boldsymbol{\beta}^{(t-1)} + \gamma_t \nabla_{\boldsymbol{\beta}} l(\boldsymbol{\beta}^{(t-1)})] - \hat{\boldsymbol{\beta}} \right\|^2 < +\infty$ by Assumption 2. For $\eta_t^{(1)}$, we have $\|\eta_t^{(1)}\|^2 \leq 2C_1(n + N)$. Since $\sum_{t=1}^{+\infty} \gamma_t^2 < +\infty$, $S^{(1)} < +\infty$. Accordingly, (15) converges a.s.

Therefore, the series in (11), (12), and (13) converge a.s, and Theorem 2 in [Atchade et al. \(2017\)](#) holds in our case. Hence, $(\boldsymbol{\beta}^{(t)})_{t \in \mathbb{N}}$ converges a.s to some $\hat{\boldsymbol{\beta}} \in \underset{\boldsymbol{\beta} \in \mathcal{B}}{\operatorname{argmax}} l(\boldsymbol{\beta})$.

A.2 Additional Details on the Settings in the Simulation Study

A.2.1 True values in the simulation study

Multilevel logistic regression model. In the lower-dimensional setting with $K = 3$, the true mean vector of random effects was set to $\mu^* = (0.300, 0.872, 0.976)$. In the higher dimensional setting with $K = 10$, the true mean vector was set to $\mu^* = (0.300, 0.026, 0.679, 0.153, 0.338, 0.675, 0.670, 0.798, 0.357, 0.322)$. These values are rounded off to three decimal places. In both settings, the true values for the diagonal and off-diagonal elements of the covariance matrix Σ were set to 0.1 and 0.05, respectively.

M2PL model. The number of intercept and factor loading parameters is too large to present the specific values in the Supplementary Materials; we have provided them on the Open Science Framework: https://osf.io/3sb4t/?view_only=abd84347053a450fa88f787d168df359. In both the lower- and higher-dimensional settings, the true values for the diagonal and off-diagonal elements of correlation matrix Σ were set to 1.0 and 0.5, respectively.

A.2.2 Initial values

Multilevel logistic regression model. The initial values of latent variables were generated from the same distribution as their true values, with the sign of the initial values set to be the same as that of the corresponding true values. Thus, these initial values hold the same sign and correlational structure as their true values but have some small deviations from them. The initial values of the mean vector μ were generated by adding a Gaussian noise following normal distribution $\mathcal{N}(0, 0.49)$ to its true values. The variance of 0.49 (standard deviation is 0.7) was chosen to obtain good starting points, minimising the effect of different sensitivities of the algorithms to starting points, while avoiding the scenario where the perturbations are too small to assess the difference in convergence speed among the competitors (if starting points happen to be close to the true values, all the algorithms converge immediately after the start of the iterations). Regarding the initial value of the covariance matrix Σ , a small perturbation to its true value sometimes induces the initial value that is close to a singular matrix, which makes parameter learning in the beginning of the iterations significantly unstable. Thus, the initial value of the covariance matrix was set to the identity matrix to avoid such a scenario across replications.

M2PL model. Similarly, the initial values of latent variables were generated from the same distribution as their true values, and the sign of the initial values were set to the same as that of the corresponding true values. The initial values of intercept d_j and factor loading \mathbf{a}_j were generated by adding a Gaussian noise following normal distribution $\mathcal{N}(0, 0.49)$ to its true values.

In order to align with the multilevel logistic regression model, we also set the initial value of the correlation matrix Σ to be the identity matrix.

A.2.3 Candidate values of the constant factors for step sizes and the random walk step size

We consider the following candidate values of the constant factors for the step sizes in the D-SOUL and SOUL algorithms: $\mu_1 = \{0.05, 0.5, 1.0, 2.5, 5.0\}$, and $\mu_2 = \{0.01, 0.02, 0.03, 0.04, 0.05\}$. In addition, the random walk step size corresponds to the standard deviation of Gaussian noise ϵ with normal distribution $\mathcal{N}(0, \sigma^2)$, and the SOMH algorithm generates a proposed latent variable by $\tilde{\xi}_{ik} = \xi_{ik}^{(t-1)} + \epsilon$, where $\tilde{\xi}_{ik}$ is the k -th dimension of the proposed value of latent variables, and $\xi_{ik}^{(t-1)}$ is the k -th dimension of the value of latent variables sampled in the previous iteration. Accordingly, we consider the random walk step size candidate values: $\sigma^2 = \{0.1, 0.2, 0.3, 0.4, 0.5\}$.

Subsequently, we ran all the algorithms for 20 data passes given different candidate values under each simulation condition for three simulated datasets. Then, we evaluated the $\text{MAE}_{\text{Multilevel}}$ or MAE_{M2PL} for each simulation condition using three simulated datasets, whose values were computed based on the model parameters updated at the last iteration. Finally, we selected the step sizes that provided the lowest $\text{MAE}_{\text{Multilevel}}$ or MAE_{M2PL} for the relevant condition. The same criteria for selecting $\mathbf{D}^{(t)}$ as in simulation study were applied to all the algorithms. Table 2 shows the step sizes chosen from the candidate values.

Table 2: Selected step sizes

	Multilevel Logistic Regression Model				Confirmatory M2PL model			
	$K = 3$		$K = 10$		$K = 3$		$K = 10$	
	μ_1	μ_2, σ^2	μ_1	μ_2, σ^2	μ_1	μ_2, σ^2	μ_1	μ_2, σ^2
D-SOUL ($n = 10$)	5.0	0.05	0.5	0.04	0.5	0.05	1.0	0.03
D-SOUL ($n = 50$)	1.0	0.05	5.0	0.04	2.5	0.05	5.0	0.03
D-SOUL ($n = 100$)	5.0	0.05	5.0	0.04	5.0	0.05	5.0	0.03
SOUL	5.0	0.05	5.0	0.01	5.0	0.03	5.0	0.01
SOMH	5.0	0.2	5.0	0.1	5.0	0.4	5.0	0.1

Note. In the column of μ_2, σ^2 , the value presented in the row of ‘‘SOMH’’ is the random walk step size σ^2 .

A.3 The Error Trajectory of the MAE for Different Model Parameters

Multilevel logistic regression model. Here, we present the error trajectory of the MAE for each parameter of the multilevel logistic regression model.

Multilevel logistic regression model with $K=3$: Mean vector

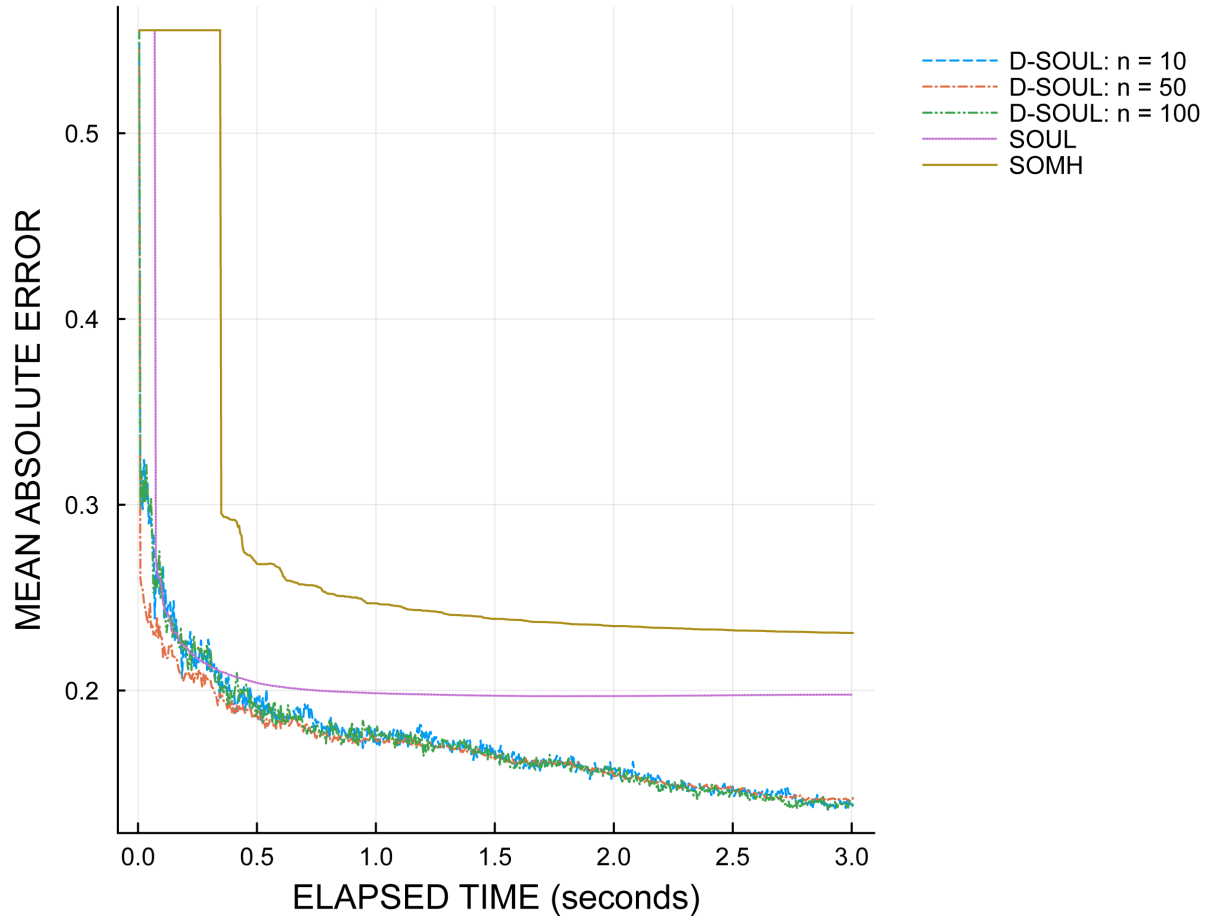


Figure 6: Error trajectory of a mean vector as a function of elapsed time: the multilevel logistic regression model with $K = 3$. The blue-dash, red-dashdot, green-dashdotdot, purple-dot, and brown-solid lines denote the trajectories from the D-SOUL algorithms with $n = 10, 50, 100$, SOUL, and SOHM algorithms, respectively.

Multilevel logistic regression model with $K=3$: Covariance matrix

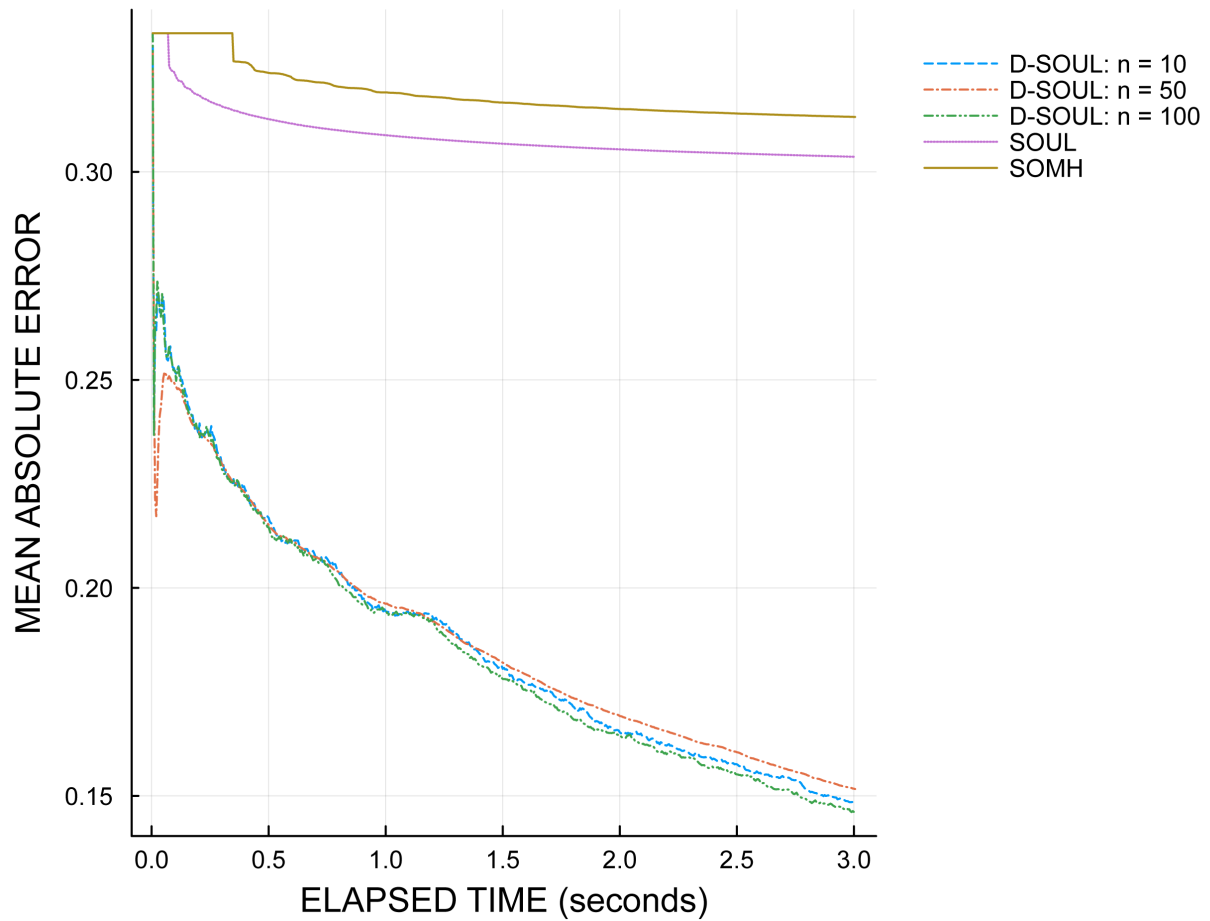


Figure 7: Error trajectory of a covariance matrix as a function of elapsed time: the multilevel logistic regression model with $K = 3$. The blue-dash, red-dashdot, green-dashdotdot, purple-dot, and brown-solid lines denote the trajectories from the D-SOUL algorithms with $n = 10, 50, 100$, SOUL, and SOHM algorithms, respectively.

Multilevel logistic regression model with $K=10$: Mean vector

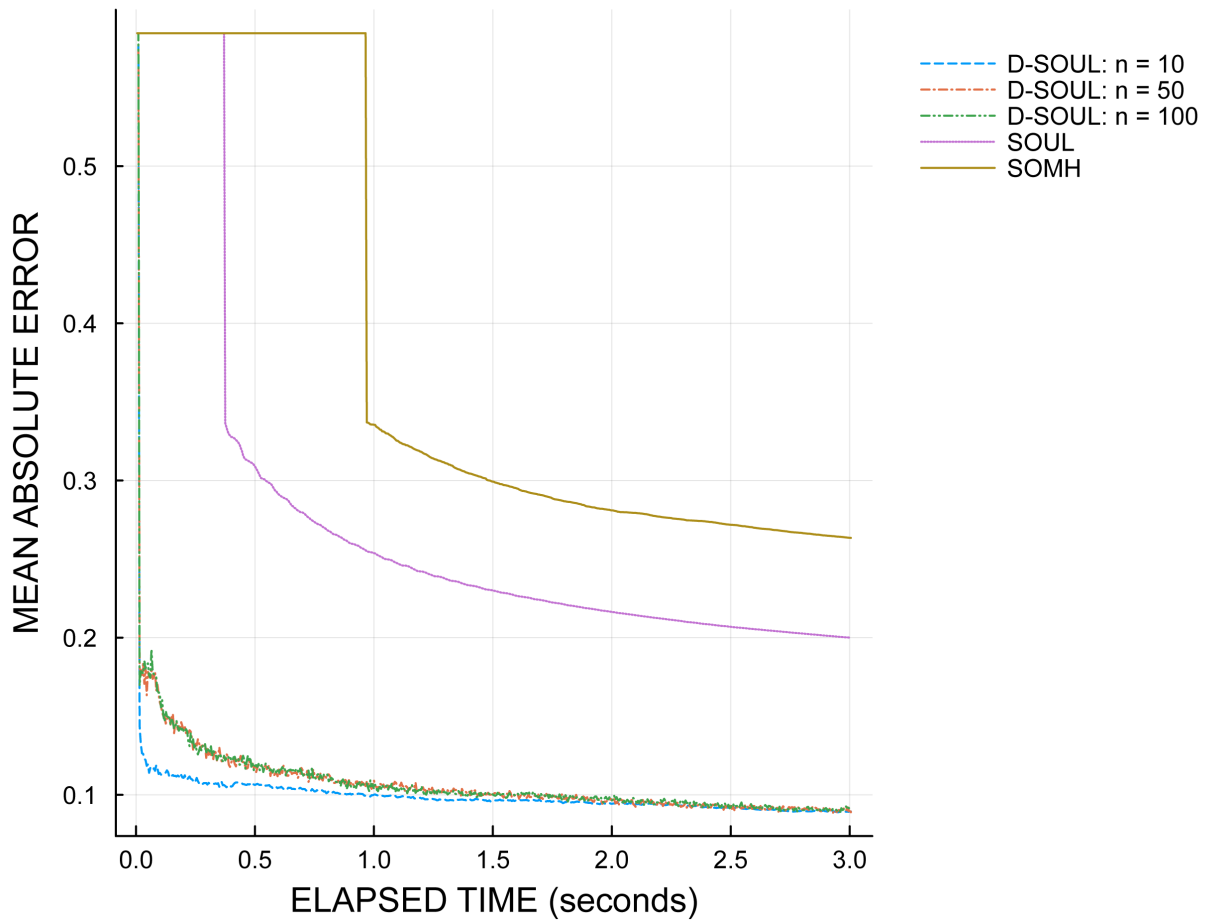


Figure 8: Error trajectory of a mean vector as a function of elapsed time: the multilevel logistic regression model with $K = 10$. The blue-dash, red-dashdot, green-dashdotdot, purple-dot, and brown-solid lines denote the trajectories from the D-SOUL algorithms with $n = 10, 50, 100$, SOUL, and SOHM algorithms, respectively.

Multilevel logistic regression model with $K=10$: Covariance matrix

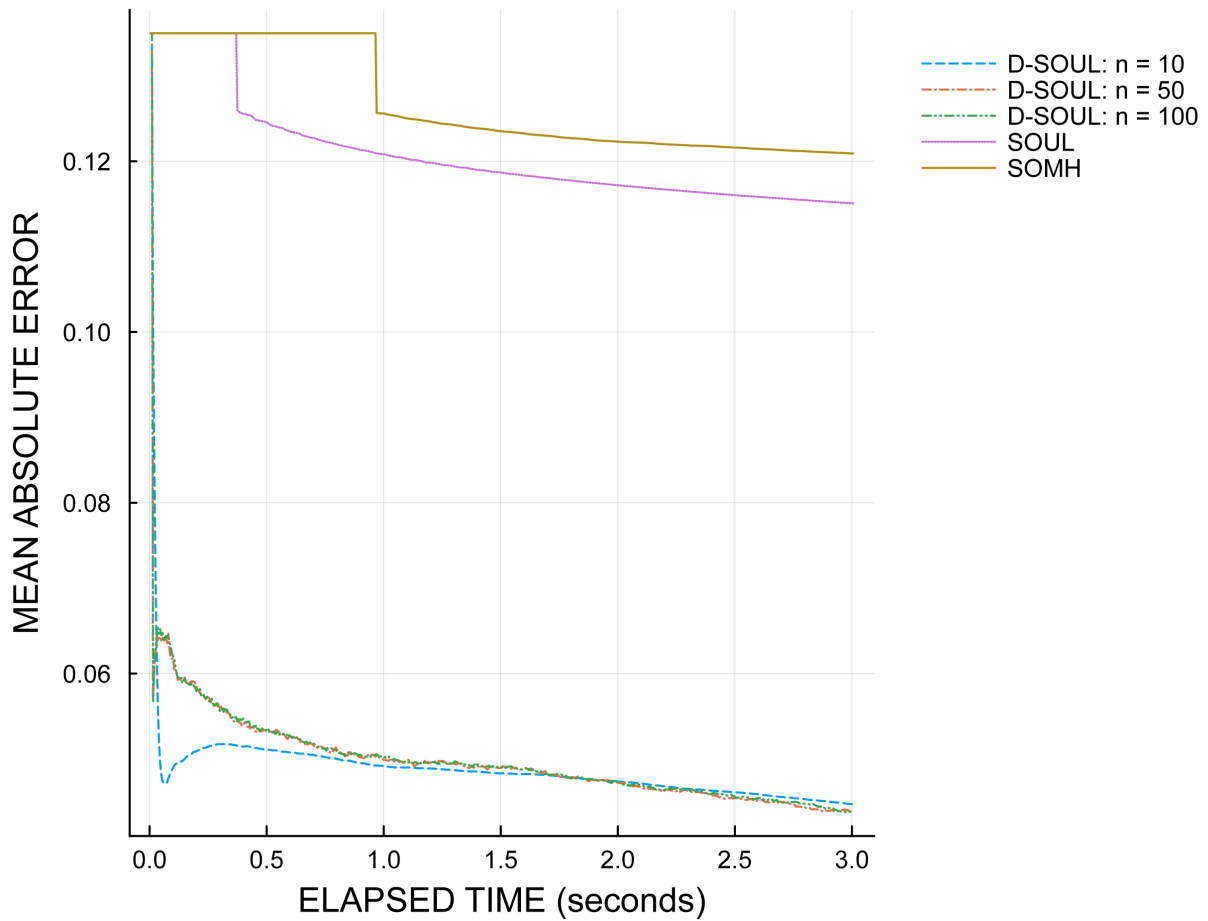


Figure 9: The error trajectory of a covariance matrix as a function of elapsed time: the multilevel logistic regression model with $K = 10$. The blue-dash, red-dashdot, green-dashdotdot, purple-dot, and brown-solid lines denote the trajectories from the D-SOUL algorithms with $n = 10, 50, 100$, SOUL, and SOHM algorithms, respectively.

M2PL model. Next, we present the error trajectory of the MAE for each parameter of the confirmatory M2PL model.

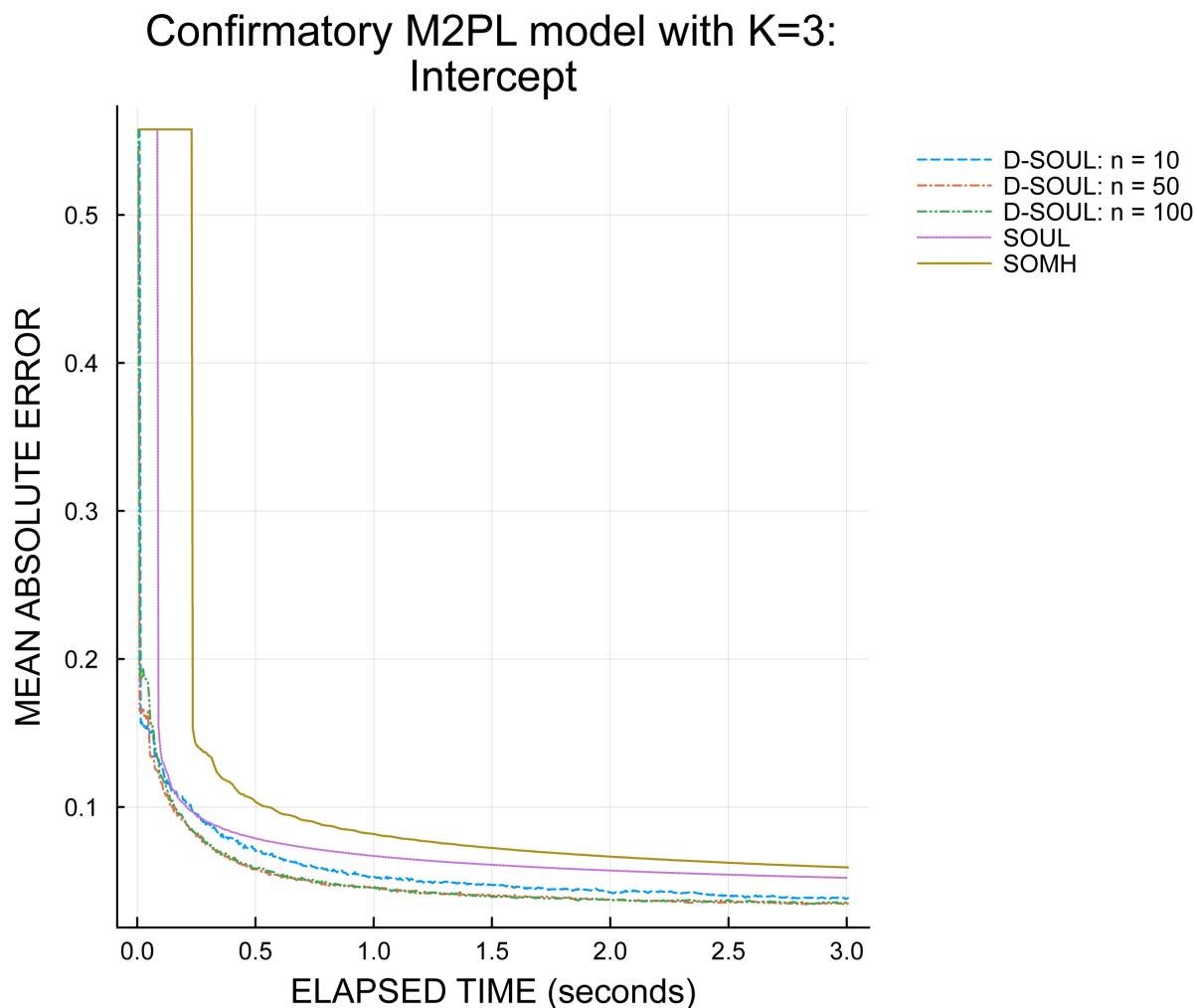


Figure 10: Error trajectory of an intercept parameter as a function of elapsed time: the confirmatory M2PL model with $K = 3$. The blue-dash, red-dashdot, green-dashdotdot, purple-dot, and brown-solid lines denote the trajectories from the D-SOUL algorithms with $n = 10, 50, 100$, SOUL, and SOHM algorithms, respectively.

Confirmatory M2PL model with $K=3$: Factor loadings

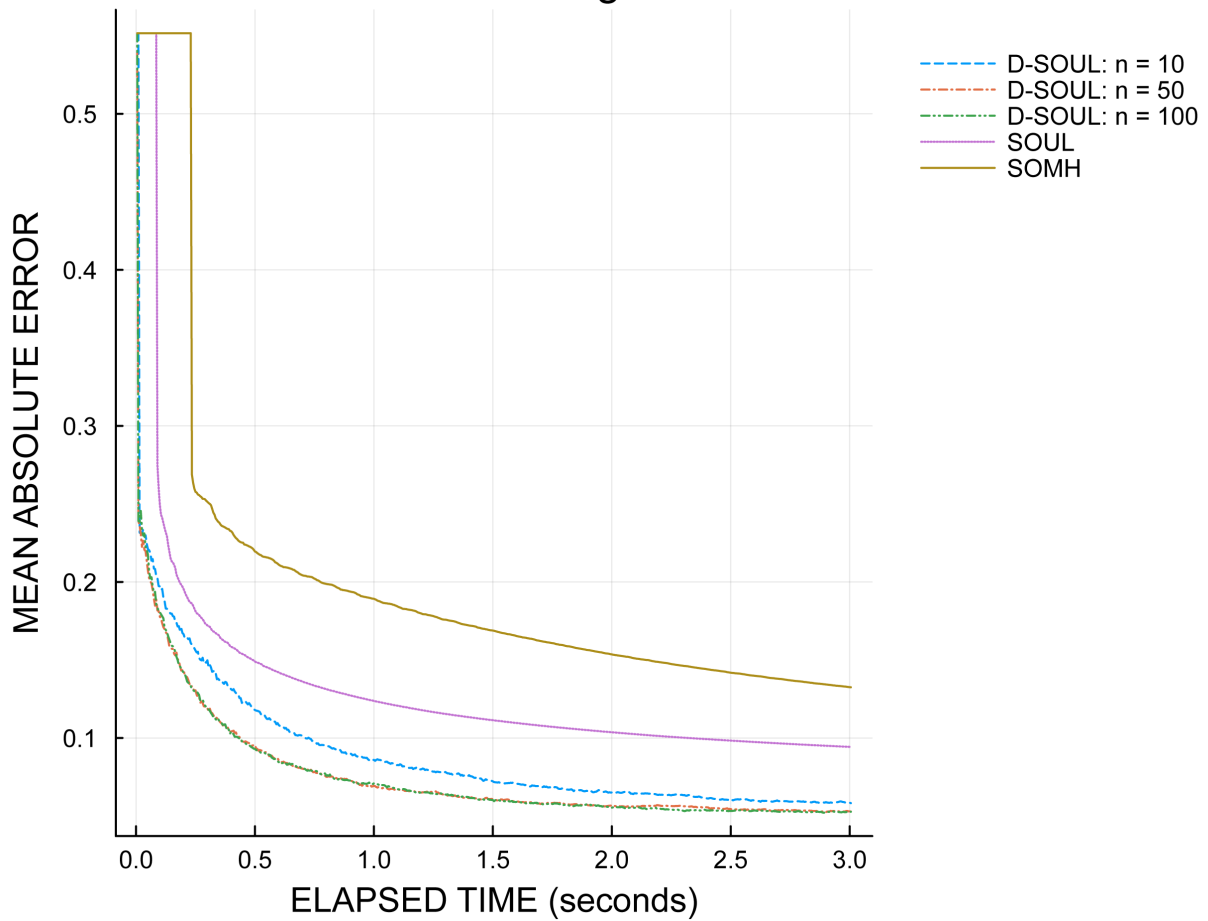


Figure 11: Error trajectory of a factor loading parameter as a function of elapsed time: the confirmatory M2PL model with $K = 3$. The blue-dash, red-dashdot, green-dashdotdot, purple-dot, and brown-solid lines denote the trajectories from the D-SOUL algorithms with $n = 10, 50, 100$, SOUL, and SOHM algorithms, respectively.

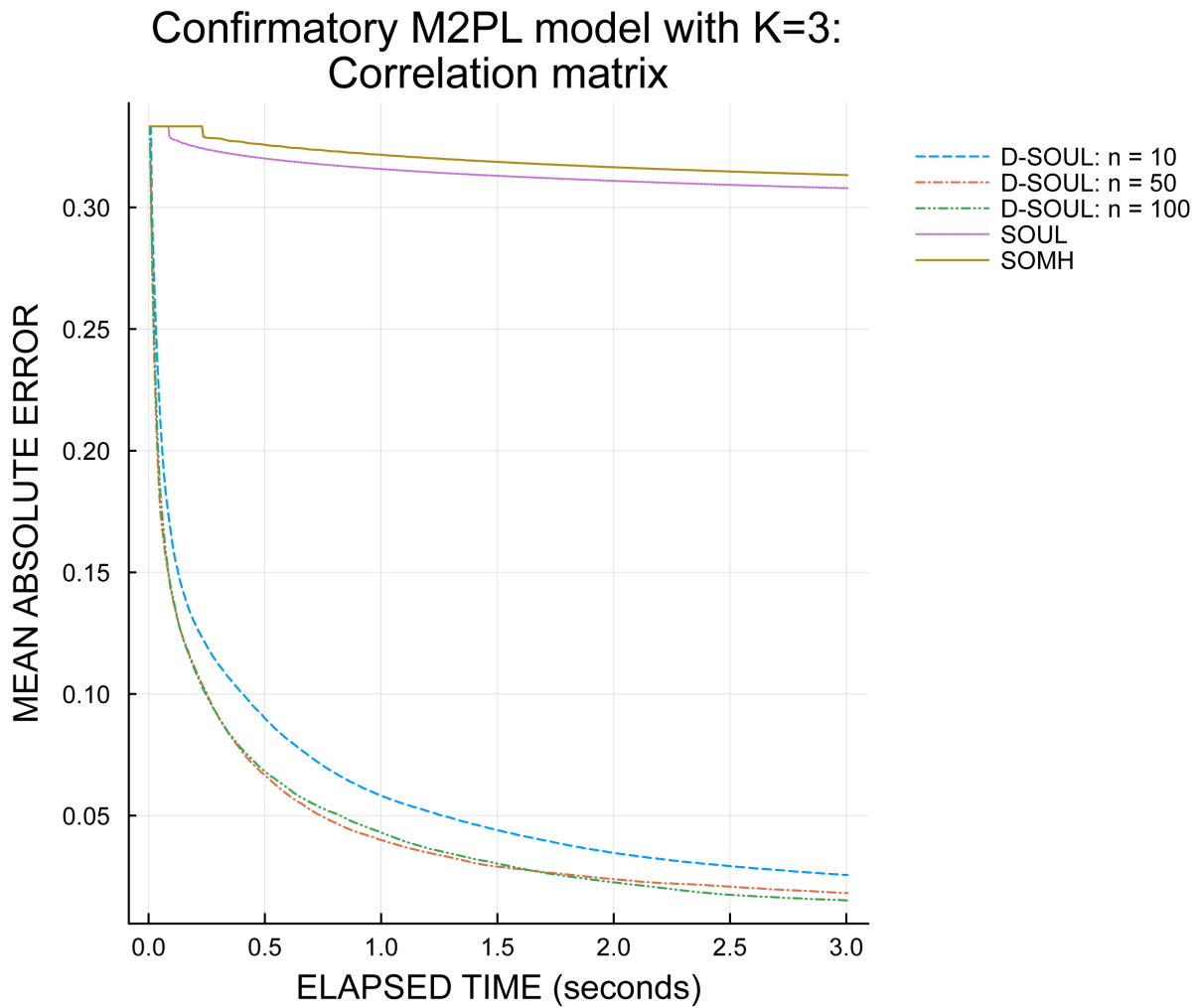


Figure 12: Error trajectory of a correlation matrix as a function of elapsed time: the confirmatory M2PL model with $K = 3$. The blue-dash, red-dashdot, green-dashdotdot, purple-dot, and brown-solid lines denote the trajectories from the D-SOUL algorithms with $n = 10, 50, 100$, SOUL, and SOHM algorithms, respectively.

Confirmatory M2PL model with $K=10$: Intercept

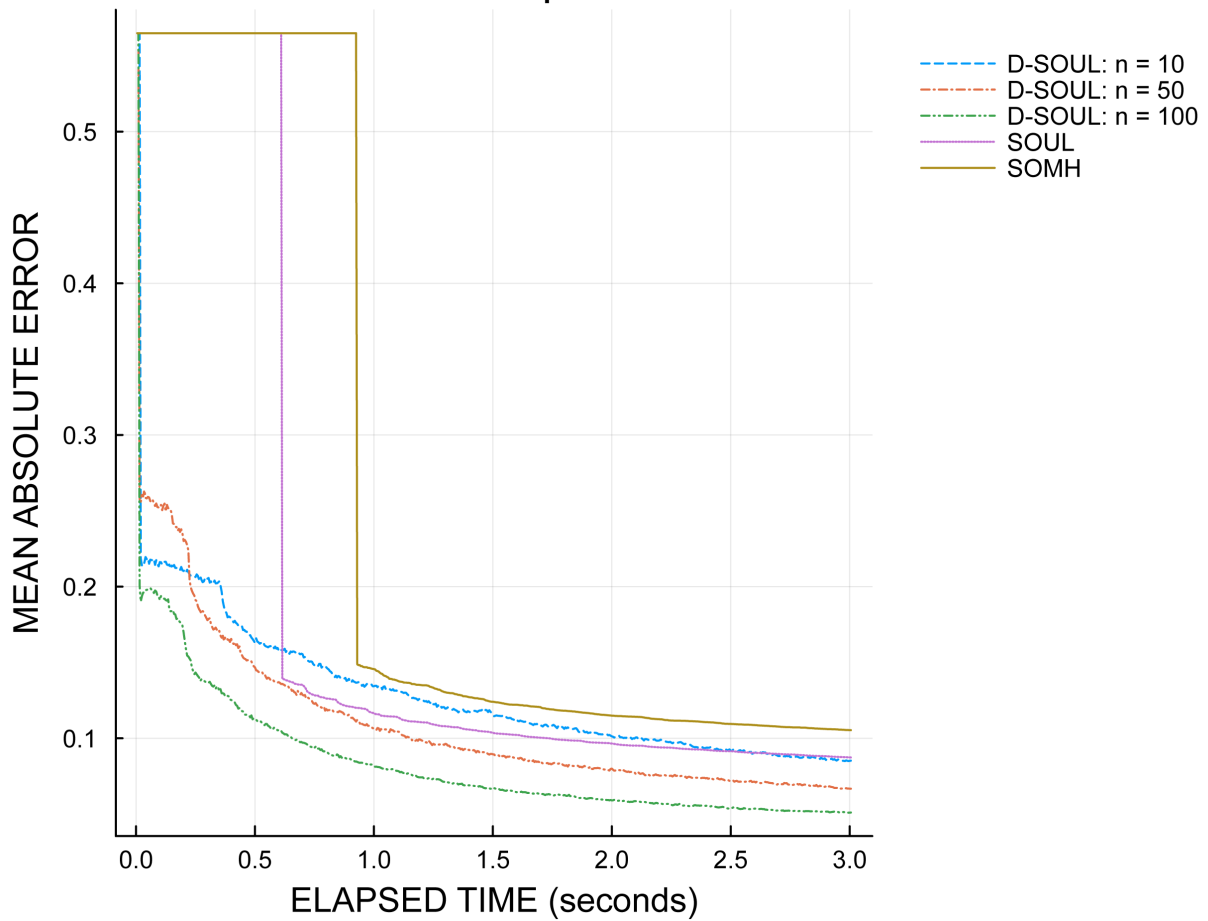


Figure 13: Error trajectory of an intercept parameter as a function of elapsed time: the confirmatory M2PL model with $K = 10$. The blue-dash, red-dashdot, green-dashdotdot, purple-dot, and brown-solid lines denote the trajectories from the D-SOUL algorithms with $n = 10, 50, 100$, SOUL, and SOHM algorithms, respectively.

Confirmatory M2PL model with $K=10$: Factor loadings

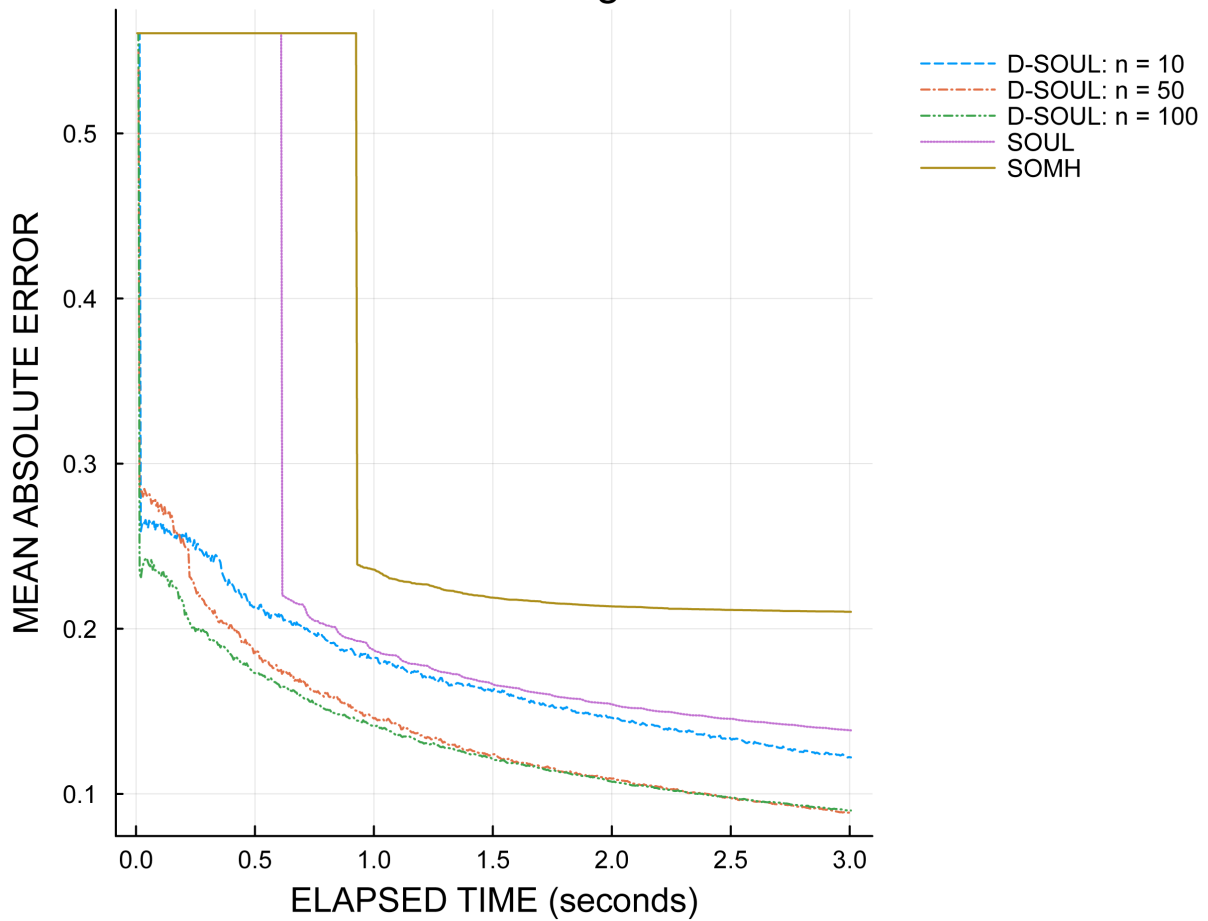


Figure 14: Error trajectory of a factor loading parameter as a function of elapsed time: the confirmatory M2PL model with $K = 10$. The blue-dash, red-dashdot, green-dashdotdot, purple-dot, and brown-solid lines denote the trajectories from the D-SOUL algorithms with $n = 10, 50, 100$, SOUL, and SOHM algorithms, respectively.

Confirmatory M2PL model with $K=10$:
Correlation matrix

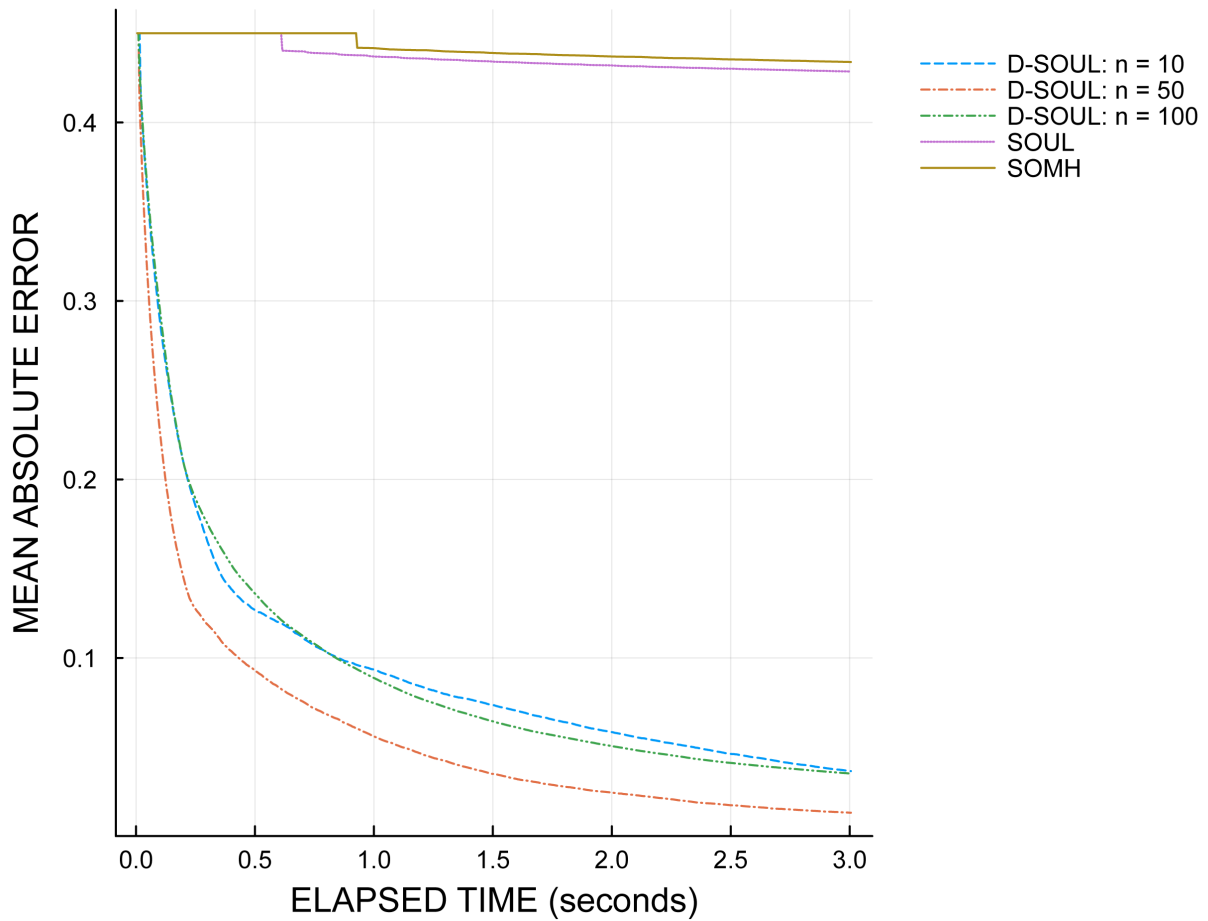


Figure 15: Error trajectory of a correlation matrix as a function of elapsed time: the confirmatory M2PL model with $K = 10$. The blue-dash, red-dashdot, green-dashdotdot, purple-dot, and brown-solid lines denote the trajectories from the D-SOUL algorithms with $n = 10, 50, 100$, SOUL, and SOHM algorithms, respectively.

A.4 Trajectory of Updated Model Parameters in the Empirical Study

Figures 16, 17, and 18 show the trajectories of the intercept and factor loading parameters and correlation matrix of the confirmatory M2PL model in the empirical study. The figures include the trajectories from both the initialisation and subsequent stages of parameter estimation. As shown in the figures, all model parameters converged.

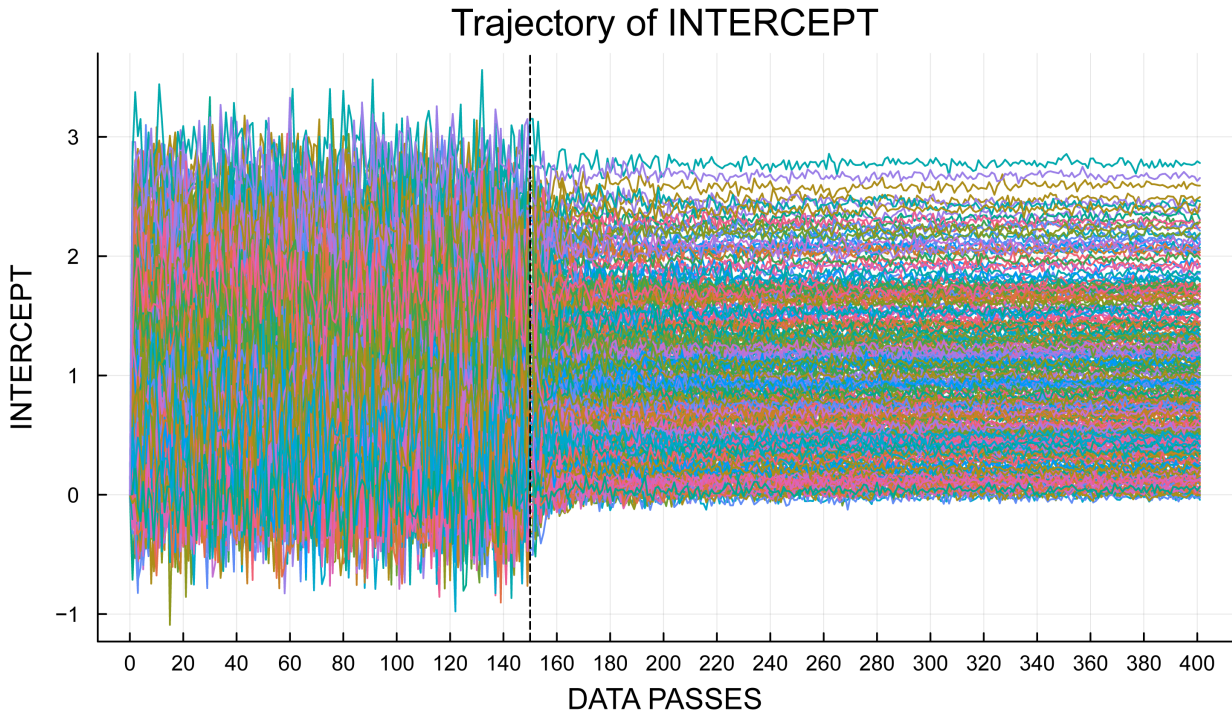


Figure 16: Trajectory of the intercept parameters for the confirmatory M2PL model. The black-dot line denotes the end of the initialisation stage.

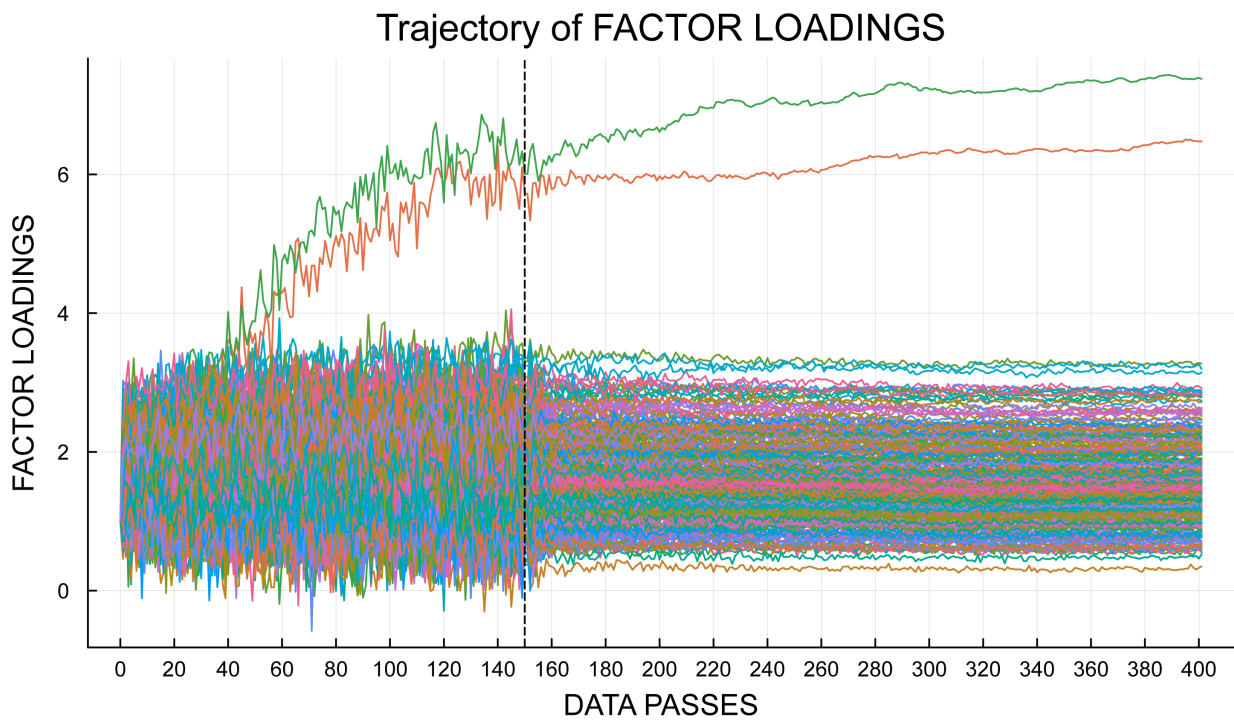


Figure 17: Trajectory of the factor loading parameters for the confirmatory M2PL model. The black-dot line denotes the end of the initialisation stage.

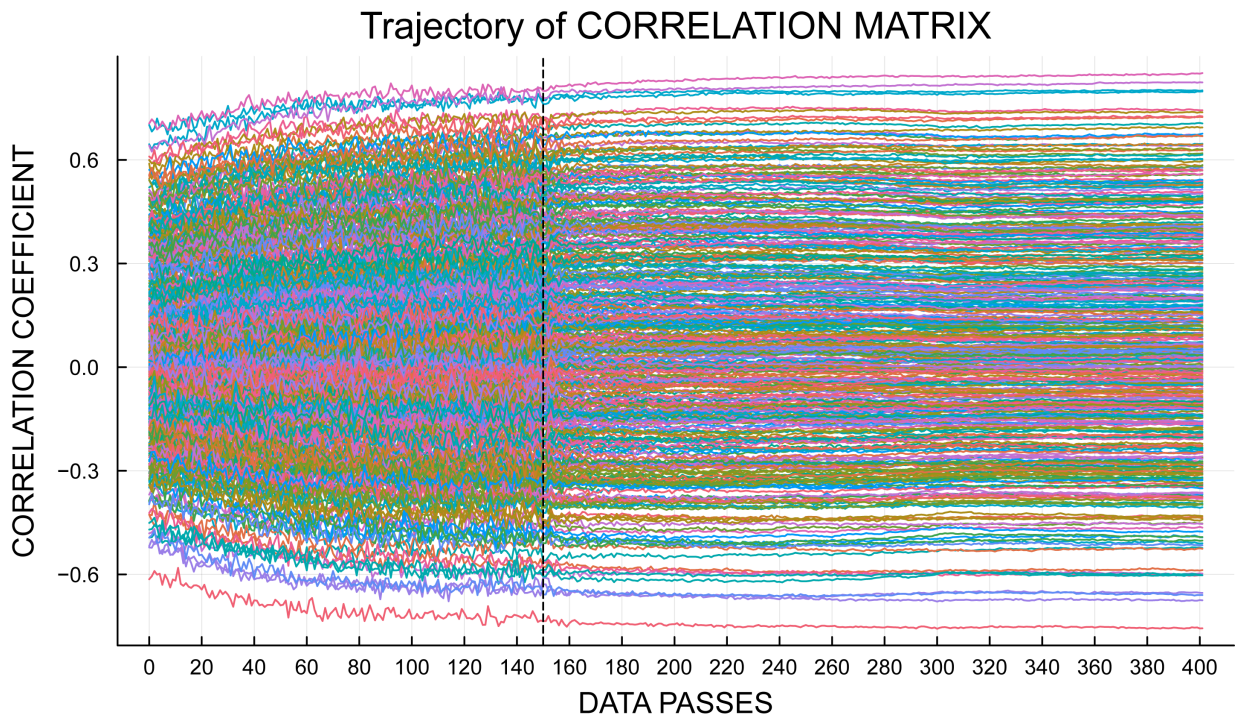


Figure 18: Trajectory of the correlation matrix of latent factors for the confirmatory M2PL model. The black-dot line denotes the end of the initialisation stage.

References

- Airoldi, E. M., Blei, D. M., Erosheva, E. A., & Fienberg, S. E. (2015). *Handbook of mixed membership models and their applications*. CRC Press.
- Andersson, B., Jin, S., & Zhang, M. (2023). Fast estimation of multiple group generalized linear latent variable models for categorical observed variables. *Computational Statistics & Data Analysis*, *182*, 1–12. <https://doi.org/10.1016/j.csda.2023.107710>
- Andersson, B., & Xin, T. (2021). Estimation of latent regression item response theory models using a second-order Laplace approximation. *Journal of Educational and Behavioral Statistics*, *46*(2), 244–265. <https://doi.org/10.3102/1076998620945199>
- Asi, H., & Duchi, J. C. (2019). The importance of better models in stochastic optimization. *Proceedings of the National Academy of Sciences*, *116*(46), 22924–22930. <https://doi.org/10.1073/pnas.1908018116>
- Atchade, Y. F., Fort, G., & Moulines, E. (2017). On perturbed proximal gradient algorithms. *Journal of Machine Learning Research*, *18*, 1–33. <https://jmlr.org/papers/volume18/15-038/15-038.pdf>
- Bartholomew, D. J., Steele, F., Galbraith, J., & Moustaki, I. (2008). *Analysis of multivariate social science data*. CRC Press.
- Bezanson, J., Edelman, A., Karpinski, S., & Shah, V. B. (2017). Julia: A fresh approach to numerical computing. *SIAM Review*, *59*(1), 65–98. <https://doi.org/10.1137/141000671>
- Bock, R. D., & Aitkin, M. (1981). Marginal maximum likelihood estimation of item parameters: Application of an EM algorithm. *Psychometrika*, *46*(4), 443–459. <https://doi.org/10.1007/BF02293801>
- Cai, L. (2010a). High-dimensional exploratory item factor analysis by a Metropolis–Hastings Robbins–Monro Algorithm. *Psychometrika*, *75*(1), 33–57. <https://doi.org/10.1007/s11336-009-9136-x>
- Cai, L. (2010b). Metropolis-Hastings Robbins-Monro algorithm for confirmatory item factor analysis. *Journal of Educational and Behavioral Statistics*, *35*(3), 307–335. <https://doi.org/10.3102/1076998609353115>
- Chen, Y., Li, X., & Zhang, S. (2019). Joint maximum likelihood estimation for high-dimensional exploratory item factor analysis. *Psychometrika*, *84*(1), 124–146. <https://doi.org/10.1007/s11336-018-9646-5>
- Chen, Y., Li, X., & Zhang, S. (2020). Structured latent factor analysis for large-scale data: Identifiability, estimability, and their implications. *Journal of the American Statistical Association*, *115*(532), 1756–1770. <https://doi.org/10.1080/01621459.2019.1635485>

- Chen, Y., & Zhang, S. (2020). A latent Gaussian process model for analysing intensive longitudinal data. *British Journal of Mathematical and Statistical Psychology*, *73*(2), 237–260. <https://doi.org/10.1111/bmsp.12180>
- Chow, S.-M., Lu, Z., Sherwood, A., & Zhu, H. (2016). Fitting nonlinear ordinary differential equation models with random effects and unknown initial conditions using the stochastic approximation Expectation–Maximization (SAEM) algorithm. *Psychometrika*, *81*(1), 102–134. <https://doi.org/10.1007/s11336-014-9431-z>
- De Bortoli, V., Durmus, A., Pereyra, M., & Vidal, A. F. (2021). Efficient stochastic optimisation by unadjusted Langevin Monte Carlo: Application to maximum marginal likelihood and empirical Bayesian estimation. *Statistics and Computing*, *31*(3), 1–18. <https://doi.org/10.1007/s11222-020-09986-y>
- Dempster, A. P., Laird, N. M., & Rubin, D. B. (1977). Maximum likelihood from incomplete data via the *EM* algorithm. *Journal of the Royal Statistical Society: Series B (Methodological)*, *39*(1), 1–22. <https://doi.org/10.1111/j.2517-6161.1977.tb01600.x>
- Diebolt, J., & Ip, E. H. (1995). Stochastic EM: Method and application. In *Markov chain Monte Carlo in practice*. CRC Press.
- Durmus, A., & Moulines, É. (2019). High-dimensional Bayesian inference via the unadjusted Langevin algorithm. *Bernoulli*, *25*(4A), 2854–2882. <https://doi.org/10.3150/18-BEJ1073>
- Edwards, M. C. (2010). A Markov chain Monte Carlo approach to confirmatory item factor analysis. *Psychometrika*, *75*(3), 474–497.
- Erosheva, E., Fienberg, S., & Lafferty, J. (2004). Mixed-membership models of scientific publications. *Proceedings of the National Academy of Sciences*, *101*(suppl_1), 5220–5227. <https://doi.org/10.1073/pnas.0307760101>
- Goodfellow, I., Bengio, Y., & Courville, A. (2016). *Deep learning* [<http://www.deeplearningbook.org>]. MIT Press.
- Gu, M. G., & Kong, F. H. (1998). A stochastic approximation algorithm with Markov chain Monte-Carlo method for incomplete data estimation problems. *Proceedings of the National Academy of Sciences*, *95*(13), 7270–7274. <https://doi.org/10.1073/pnas.95.13.7270>
- Haberman, S. J. (1977). Maximum likelihood estimates in exponential response models. *The Annals of Statistics*, *5*(5), 815–841. <https://doi.org/10.1214/aos/1176343941>
- Henson, R. A., Templin, J. L., & Willse, J. T. (2009). Defining a family of cognitive diagnosis models using log-linear models with latent variables. *Psychometrika*, *74*(2), 191–210. <https://doi.org/10.1007/s11336-008-9089-5>
- Hoff, P. D., Raftery, A. E., & Handcock, M. S. (2002). Latent space approaches to social network analysis. *Journal of the American Statistical Association*, *97*(460), 1090–1098. <https://doi.org/10.1198/016214502388618906>

- Hsieh, Y.-P., Kavis, A., Rolland, P., & Cevher, V. (2018). Mirrored Langevin dynamics. In S. Bengio, H. Wallach, H. Larochelle, K. Grauman, N. Cesa-Bianchi, & R. Garnett (Eds.), *Advances in neural information processing systems* (Vol. 31). Curran Associates, Inc. https://proceedings.neurips.cc/paper_files/paper/2018/file/6490791e7abf6b29a381288cc23a8223-Paper.pdf
- Huber, P., Ronchetti, E., & Victoria-Feser, M.-P. (2004). Estimation of generalized linear latent variable models. *Journal of the Royal Statistical Society Series B: Statistical Methodology*, *66*(4), 893–908. <https://doi.org/10.1111/j.1467-9868.2004.05627.x>
- Jarner, S. F., & Hansen, E. (2000). Geometric ergodicity of Metropolis algorithms. *Stochastic Processes and their Applications*, *85*(2), 341–361. [https://doi.org/10.1016/S0304-4149\(99\)00082-4](https://doi.org/10.1016/S0304-4149(99)00082-4)
- Johnson, J. A. (2005). Ascertaining the validity of individual protocols from web-based personality inventories. *Journal of Research in Personality*, *39*(1), 103–129. <https://doi.org/10.1016/j.jrp.2004.09.009>
- Johnson, J. A. (2014). Measuring thirty facets of the five factor model with a 120-item public domain inventory: Development of the IPIP-NEO-120. *Journal of Research in Personality*, *51*, 78–89. <https://doi.org/10.1016/j.jrp.2014.05.003>
- Lu, Z.-H., Chow, S.-M., Sherwood, A., & Zhu, H. (2015). Bayesian analysis of ambulatory blood pressure dynamics with application to irregularly spaced sparse data. *The Annals of Applied Statistics*, *9*(3), 1601–1620. <https://doi.org/10.1214/15-AOAS846>
- Matthews, P. (1993). A slowly mixing markov chain with implications for Gibbs sampling. *Statistics & Probability Letters*, *17*(3), 231–236. [https://doi.org/10.1016/0167-7152\(93\)90172-F](https://doi.org/10.1016/0167-7152(93)90172-F)
- Meng, X.-L., & Schilling, S. (1996). Fitting full-information item factor models and an empirical investigation of bridge sampling. *Journal of the American Statistical Association*, *91*(435), 1254–1267. <https://doi.org/10.1080/01621459.1996.10476995>
- Nemirovskij, A. S., & Yudin, D. B. (1983). *Problem complexity and method efficiency in optimization*. Wiley-Interscience.
- Nielsen, S. F., & Nielsen, S. F. (2000). The stochastic EM algorithm: Estimation and asymptotic results. *Bernoulli*, *6*(3), 457–489. <https://doi.org/10.2307/3318671>
- Polyak, B. T., & Juditsky, A. B. (1992). Acceleration of stochastic approximation by averaging. *SIAM Journal on Control and Optimization*, *30*(4), 838–855. <https://doi.org/10.1137/0330046>
- Robbins, H., & Monro, S. (1951). A stochastic approximation method. *The Annals of Mathematical Statistics*, *22*(3), 400–407. <https://doi.org/10.1214/aoms/1177729586>
- Roberts, G. O., & Rosenthal, J. S. (1998). Optimal scaling of discrete approximations to Langevin diffusions. *Journal of the Royal Statistical Society Series B: Statistical Methodology*, *60*(1), 255–268. <https://doi.org/10.1111/1467-9868.00123>

- Roberts, G. O., & Tweedie, R. L. (1996). Exponential convergence of Langevin distributions and their discrete approximations. *Bernoulli*, 2(4), 341–363. <https://doi.org/10.2307/3318418>
- Ruppert, D. (1988). Efficient estimations from a slowly convergent Robbins-Monro process. *Technical Report, Cornell University Operations Research and Industrial Engineering*. <https://hdl.handle.net/1813/8664>
- Schilling, S., & Bock, R. D. (2005). High-dimensional maximum marginal likelihood item factor analysis by adaptive quadrature. *Psychometrika*, 70(3), 533–555. <https://doi.org/10.1007/s11336-003-1141-x>
- Shun, Z. (1997). Another look at the salamander mating data: A modified Laplace approximation approach. *Journal of the American Statistical Association*, 92(437), 341–349. <https://doi.org/10.1080/01621459.1997.10473632>
- Shun, Z., & McCullagh, P. (1995). Laplace Approximation of High Dimensional Integrals. *Journal of the Royal Statistical Society: Series B (Methodological)*, 57(4), 749–760. <https://doi.org/10.1111/j.2517-6161.1995.tb02060.x>
- Skrondal, A., & Rabe-Hesketh, S. (2004). *Generalized latent variable modeling: Multilevel, longitudinal, and structural equation models*. Chapman & Hall/CRC.
- Von Davier, M., & Yamamoto, K. (2004). Partially observed mixtures of IRT models: An extension of the generalized partial-credit model. *Applied Psychological Measurement*, 28(6), 389–406. <https://doi.org/10.1177/0146621604268734>
- Wei, G. C. G., & Tanner, M. A. (1990). A monte carlo implementation of the EM algorithm and the poor man’s data augmentation algorithms. *Journal of the American Statistical Association*, 85(411), 699–704. <https://doi.org/10.1080/01621459.1990.10474930>
- Zanella, G. (2020). Informed proposals for local MCMC in discrete spaces. *Journal of the American Statistical Association*, 115(530), 852–865. <https://doi.org/10.1080/01621459.2019.1585255>
- Zhang, A., Lipton, Z., Li, M., & Smola, A. J. (2024). *Dive into deep learning*. Cambridge University Press. <https://doi.org/10.1017/9781009389426>
- Zhang, R., Liu, X., & Liu, Q. (2022). A Langevin-like sampler for discrete distributions. In K. Chaudhuri, S. Jegelka, L. Song, C. Szepesvari, G. Niu, & S. Sabato (Eds.), *Proceedings of the 39th international conference on machine learning* (pp. 26375–26396, Vol. 162). PMLR. <https://proceedings.mlr.press/v162/zhang22t.html>
- Zhang, S., & Chen, Y. (2022). Computation for latent variable model estimation: A unified stochastic proximal framework. *Psychometrika*, 87(4), 1473–1502. <https://doi.org/10.1007/s11336-022-09863-9>
- Zhang, S., Chen, Y., & Liu, Y. (2020). An improved stochastic EM algorithm for large-scale full-information item factor analysis. *British Journal of Mathematical and Statistical Psychology*, 73(1), 44–71. <https://doi.org/10.1111/bmsp.12153>

Zhu, Y., Shen, X., & Ye, C. (2016). Personalized prediction and sparsity pursuit in latent factor models. *Journal of the American Statistical Association*, 111(513), 241–252. <https://doi.org/10.1080/01621459.2014.999158>